[redacted] E-7607-4 (Memo) 649

NASA TM X-250



# TECHNICAL MEMORANDUM

X-250

## PRELIMINARY INVESTIGATION OF OFF-DESIGN PERFORMANCE OF DIVERGENT-EJECTOR-TYPE ROCKET NOZZLES

By Laurence W. Gertsma and Richard A. Yeager

Lewis Research Center
Cleveland, Ohio



[redacted]



NATIONAL AERONAUTICS AND SPACE ADMINISTRATION
WASHINGTON
March 1960

[redacted]

NATIONAL AERONAUTICS AND SPACE ADMINISTRATION

TECHNICAL MEMORANDUM X-250

# PRELIMINARY INVESTIGATION OF OFF-DESIGN PERFORMANCE OF DIVERGENT-EJECTOR-TYPE ROCKET NOZZLES*

By Laurence W. Gertsma and Richard A. Yeager

## SUMMARY

An investigation was conducted to determine off-design performance levels obtainable for ejector-type rocket nozzles having design pressure ratios of 361. The nozzles were operated in a Mach 2.0 airstream to obtain a low base pressure. The resulting effective pressure ratio (jet total to base static) ranged up to 165.

With small amounts of secondary airflow, ejector wall pressure distributions indicated that overexpansion of the primary flow was prevented. As a result, the ejectors provide about 15 percent more thrust at lift-off than an equivalent 361 convergent-divergent nozzle, thus giving good low-altitude performance while retaining the advantages of a high-pressure-ratio nozzle at high altitude.

The data were used to calculate nozzle performance over a typical booster flight path. The results showed that the average thrust of the ejector with the bell primary nozzle was always higher than that of a convergent-divergent nozzle with a design pressure ratio of 89.5. If the convergent-divergent nozzle thrust was penalized by the difference in base drag, the average thrust of the ejector with bell primary nozzle was about 3.4 percent higher than that of the convergent-divergent nozzle at the end of 130 seconds.

## INTRODUCTION

A booster rocket motor usually must operate from sea level to altitudes over 100,000 feet. Thus, the propulsive nozzle experiences large changes in pressure ratio. Typical values vary from 40 at takeoff to in excess of 4000 at burnout. If the nozzle is of the usual fixed convergent-divergent type, it is on design at only one instant during a given flight; consequently, off-design performance is an important factor in the overall or integrated performance.

*Title, Unclassified.

One nozzle type that has shown good performance at lower than design pressure ratios is the divergent ejector. At these pressure ratios the low-energy secondary air prevents overexpansion of the main jet, and good performance can be obtained. The factors affecting ejector performance have received some attention for the turbojet case (i.e., for pressure ratios from 10 to 30 (see, e.g., refs. 1 and 2)), but little work has been done in the pressure-ratio range of rocket booster engines.

In view of the good performance obtained for these turbojet systems, an investigation was conducted to determine off-design performance levels obtainable for ejector nozzles having design pressure ratios near 360, this value being in the range of interest for rocket boosters. Parameters investigated were primary-nozzle shape (conical and bell), secondary-throat area, and shroud axial location. The primary-nozzle design pressure ratio was fixed at 50.

By running the models in the NASA Lewis 8- by 6-foot supersonic tunnel at Mach 2.0, sufficiently low base pressures were generated to produce "effective" pressure ratios (ratio of jet total pressure to local base region static pressure) up to 165. Unheated air was used for both the main jet and the secondary flow.

## MODEL

A schematic diagram of the model is shown in figure 1. Air was supplied to the model by a 120-pound-per-square-inch line through wing struts just forward of the section shown. The primary total pressure was measured by a 17-tube total-pressure rake located in an area of low Mach number downstream of a set of straightening vanes. The secondary total pressure was measured by two 3-tube rakes at the secondary throat. The area of the secondary throat was varied by the use of inserts in the ejector shroud. The relative location of the shroud (i.e., the distance from the primary exit to the ejector exit) was changed by adjusting the length of the upstream portion of the primary nozzle.

The photograph of the model (fig. 2) shows the rows of static-pressure taps in both the primary nozzle and ejector along with the position of one of the secondary total-pressure rakes. The rake was set to one side of the row of static taps so that it would not interfere with the static-pressure measurements. The base pressure was measured by four static-pressure taps located on the base annulus of the ejector shroud.

Two primary nozzles, a conical and a bell shape, were used. Both had a design pressure ratio of 50 ($d_p/d_t = 2.26$, see fig. 3(b)). (Symbols are defined in appendix A.) The bell nozzle was obtained by cutting

back an isentropic nozzle designed for a pressure ratio of 100; the resulting wall angle at the exit was 5°.

The shrouds were designed for a pressure ratio of 361 ($d_e/d_t = 4.38$). The method used to obtain the shroud designs was as follows: The shroud exit angle was chosen to be 8° (see sketch (a)). An arbitrary curve was

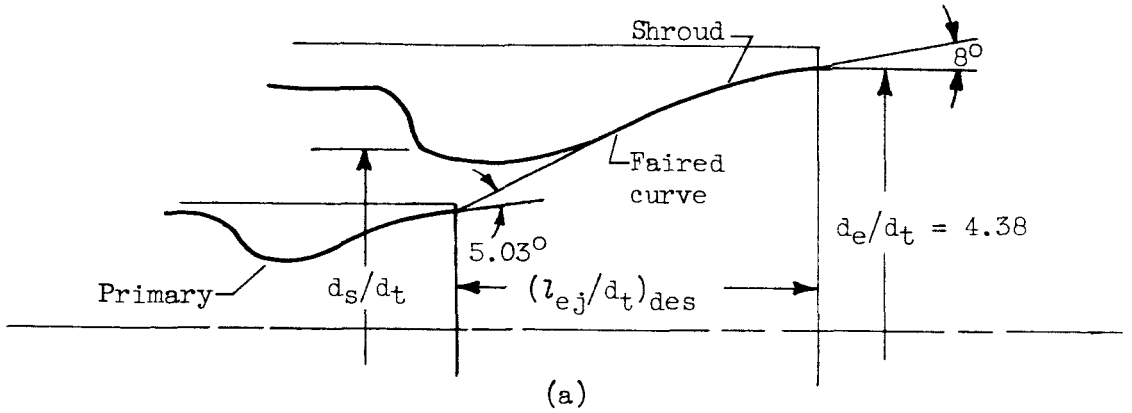


(a)

faired between the 8° exit angle and a line drawn from the primary nozzle having an angle of 5.03° greater than that of the primary exit [$5.03° = 1/4(\nu_{361} - \nu_{50})$, where $\nu$ is the Prandtl-Meyer angle]. The shroud contour near the throat was obtained by fairing from the curve to the desired value of $d_s/d_t$. This procedure also provided a design shroud length, $l_{ej}/d_t$. Values for $d_s/d_t$ were 3.25 and 2.82. Shroud contours are shown in figure 3(a).

## PROCEDURE AND DATA REDUCTION

Data were taken by setting the primary pressure and then varying the secondary pressure over a range of values. The weight flows were measured with standard ASME thin-plate, flange-tap orifices. The shroud length $l_{ej}/d_t$ was varied from the design value to values less than design. Thrust values were obtained by nozzle wall pressure integration and upstream momentum obtained from the rake stations. The methods of thrust calculation are explained in detail in appendix B.

## RESULTS AND DISCUSSION

The discussion is divided into two parts. In the first, the basic data on ejector pumping and thrust as obtained in the tunnel are presented. The second part is an estimation of the performance for a typical missile flight path.

## Basic Data

Pumping. - Both the experimental and the theoretical pumping characteristics of the ejector shroud are presented in figure 4 for the two secondary-throat areas. The experimental curve was obtained by fairing a curve through data obtained from the various configurations. The theoretical curves are based mainly on the assumption that choking occurs in the secondary throat. (Details are explained in appendix C.) At near-zero weight-flow ratio, the experimental pressure ratio is lower than the theoretical. At all other points, the experimental pressure ratio is higher than theoretical, indicating that the secondary flow was actually choked downstream of the secondary throat by the expansion of the primary jet.

Thrust. - Basic thrust performance data are included in figures 5 and 6. The curves are included only to present the data from which the significant results of this report were computed. Since, for these figures, both the actual and ideal thrusts are based on unreasonably low jet pressure ratios ($(P_p/p_0)_{max} \approx 30$), thrust ratios are quite low. In the section that follows, the more significant thrust calculations based on the higher pressure ratio (effective jet press. ratio, $P_p/p_b$) will be discussed.

Pressure distributions. - Ejector wall pressure distributions for some typical operating conditions are presented in figures 7 and 8. For completely attached primary flow and zero secondary flow, the static- to total-pressure ratio at the exit should be 0.00277 (i.e., 1/361), but the lowest ratio reached was about 0.0045. In general, for zero or very low secondary flows, shroud pressures are below the exit pressure; that is, the flow overexpands. As secondary flow increases, the shroud pressures become uniform and are almost equal to the exit pressure. Further increase in flow causes the secondary flow itself to overexpand; and, finally, for very high flows wall pressures would be equal to or above the exit pressure.

## Calculated Quiescent-Air Performance

Calculated quiescent-air performance was obtained by replacing the free-stream static pressure $p_0$ in all the thrust computations with the base pressure $p_b$ (see appendix B). The performance curves are presented in figures 9 and 10. Thrust ratio is plotted as a function of effective secondary pressure ratio $P_s/p_b$ for several values of effective primary pressure ratio $P_p/p_b$. For systems in which the secondary fluid is taken in from the external stream, secondary pressure ratios of interest vary from 1.0 at takeoff to approximately 1.7 at Mach 1, 5 at Mach 2, and so forth.

The calculated performance of the ejector with conical primary nozzle is presented in figure 9(a) for $d_s/d_t = 2.82$, and in figure 9(b) for $d_s/d_t = 3.25$. With the small throat, the off-design position of $l_{ej}/d_t = 3.31$ had the lowest thrust; for the other shroud positions, the thrust ratios were generally grouped together. With the larger throat, the effect was reversed. Here, the thrust for $l_{ej}/d_t = 3.31$ was usually the highest. For the no-secondary-flow conditions, the thrust for the on-design position was about 5 percent lower than for the other positions. The thrust ratio for both throats was always above 0.90.



The performance of the ejector with the bell primary nozzle, $d_s/d_t = 2.82$, is presented in figure 10. For this configuration, the slightly off-design position of $l_{ej}/d_t = 4.68$ usually had a higher thrust than the other positions.

Two final comments should be made about these figures. First, the thrust ratio exceeded unity only for $P_s/p_b > 1$. Thrust ratios above unity resulted from basing the ideal thrust on the primary jet only; whereas the secondary air, which was supplied by another source, added thrust also. Secondly, the amount of data is limited at low values of $P_s/p_b$, particularly at the higher effective primary pressure ratios. This resulted from the fact that in the tunnel small amounts of secondary air caused large changes in base pressure (figs. 5 and 6).

As an example of the expected performance of the ejector nozzle in actual use, thrust calculations were made over a typical ballistic flight path, the parameters of which are presented in figure 11. The base-pressure schedule shown was obtained from various experimental sources. The computed ejector performance along this trajectory is compared to that with convergent-divergent nozzles in figures 12 and 13. The convergent-divergent nozzles chosen for comparison had design pressure ratios of 361 and 89.5. The performance of the convergent-divergent nozzles was assumed to be 2 percent less than the theoretical isentropic values. The same primary total pressure, 650 pounds per square inch absolute, and primary throat area (and therefore the same weight flow) were used for both nozzle types. For the ejectors the optimum quantity of secondary flow consistent with that available from a ram scoop inlet was used, and the free-stream momentum of the secondary was subtracted from the ejector thrust. Above Mach 1 the effective pressure ratio is greater than that for which data are available, and ejector performance was assumed to be 2.5 percent less than theoretical.

The large performance advantage at low pressure ratios resulting from the use of low-energy secondary flow is illustrated in figure 12(a). The ejectors provide about 15 percent more thrust at lift-off than a

convergent-divergent nozzle having the same design pressure ratio (i.e., 361). The thrust advantage results from the fact that small amounts of secondary flow prevent overexpansion of the primary flow. This was, of course, evident in the wall pressure distributions of figure 7.

Since the poor lift-off performance of the 361 convergent-divergent nozzle eliminates it as a choice for booster applications, the ejectors are compared with an 89.5 convergent-divergent nozzle in figure 12(b). At low speeds (or altitudes) both nozzle types have about the same thrust, the ejectors being slightly better at lift-off and the convergent-divergent nozzle having an advantage near Mach 1. The important point, however, is the large gain at higher speeds due to the greater design pressure ratio of the ejectors.

For a more realistic comparison between the ejectors and the convergent-divergent nozzle, the difference in exit area was considered (fig. 12(c)). The assumption was made that the base diameter of the vehicle would be fixed in size regardless of the nozzle used. A base-drag increment $\Delta D_b$ was computed using the difference in the exit areas of the ejector and convergent-divergent nozzle with the base-pressure schedule of figure 11. The drag increment was subtracted from the thrust of the convergent-divergent nozzle, and the results are plotted in figure 12(c). Drag reduced the performance of the convergent-divergent nozzle by a maximum of about 1.25 percent near Mach 1.5.

As a final step in the comparisons, the thrust was integrated with respect to time to obtain an average thrust up to a given time. The results of the integration are presented in figure 13. The ejector with bell primary nozzle always had a higher average thrust than the 89.5-pressure-ratio convergent-divergent nozzle. The average thrust of the ejector with conical primary nozzle exceeded that of the convergent-divergent nozzle for times greater than 85 seconds if base drag was not taken into consideration and for times greater than 70 seconds if the convergent-divergent nozzle was penalized by base drag. After 130 seconds, the difference in average thrust between the ejector with bell primary nozzle and the convergent-divergent nozzle corrected for base drag was about 3.4 percent.

## SUMMARY OF RESULTS

An investigation to determine off-design performance levels obtainable for bell and conical ejector nozzles with design pressure ratios of 361 was conducted. An effective pressure ratio (i.e., jet total/base static) ranging up to 165 was obtained at Mach 2.0.

At effective pressure ratios corresponding to low altitudes, pressure distributions showed that with small amounts of secondary air the

ejector wall pressure was nearly uniform and nearly equal to the local effective exit pressure. This indicated that overexpansion of the primary flow had been prevented. As a result, the ejectors provide about 15 percent more thrust at lift-off than an equivalent 361 convergent-divergent nozzle and about 3 percent more than a typical 89.5 convergent-divergent nozzle. Thus, the ejectors have good low-altitude performance while retaining the advantages of a high-pressure-ratio nozzle at high altitudes.



Calculated quiescent-air performance showed that changes in secondary-throat location usually had little effect for the conical nozzles. For the bell nozzle a position slightly upstream of design usually had the best thrust.

Finally, when the data were used to calculate performance over a typical booster flight path, the results showed that the average thrust of the ejector with the bell primary nozzle was always higher than that of a convergent-divergent nozzle with an 89.5 design pressure ratio. If the convergent-divergent nozzle thrust was penalized by the difference in base drag, the average thrust of the ejector with bell primary nozzle was about 3.4 percent higher than that of the convergent-divergent nozzle at the end of 130 seconds.

Lewis Research Center
National Aeronautics and Space Administration
Cleveland, Ohio, December 22, 1959

## APPENDIX A

## SYMBOLS

| | |
|---|---|
| $A$ | area |
| $A^*$ | area at Mach number 1.0 |
| $D$ | drag |
| $d$ | diameter |
| $d_s/d_t$ | ejector diameter ratio |
| $F$ | thrust |
| $F/F_{p,id}$ | thrust ratio |
| $\frac{F - m_s v_0}{F_{p,id}}$ | net-thrust ratio |
| $\frac{F - m_s v_0 - \Delta D_b}{F_{p,id}}$ | ratio of net thrust minus change in base drag |
| $h$ | altitude, ft |
| $l_{ej}$ | shroud length (from primary-nozzle exit) |
| $M$ | Mach number |
| $\mathscr{M}$ | momentum |
| $m$ | mass flow |
| $P$ | total pressure |
| $P_p/p_b$ | effective primary jet pressure ratio |
| $P_p/p_0$ | jet pressure ratio |
| $P_s/P_p$ | ejector pressure ratio |
| $P_s/p_b$ | effective secondary pressure ratio |
| $p$ | static pressure |

| | |
|---|---|
| $p_b/p_0$ | base pressure ratio |
| T | total temperature |
| t | time, sec |
| $\frac{1}{t'}\int_0^{t'} \frac{F - D}{F_{p,id}}\, dt$ | average thrust |
| v | velocity |
| w | weight flow |
| x | distance upstream of shroud exit |
| $\gamma$ | ratio of specific heats |
| $\rho$ | density |
| $\tau$ | temperature ratio, $T_s/T_p$ |
| $\omega$ | weight-flow ratio, $w_s/w_p$ |

Subscripts:

| | |
|---|---|
| b | base, ejector |
| des | design |
| e | exit |
| ej | ejector |
| id | ideal |
| max | maximum |
| p | primary stream |
| q | quiescent air |
| s | secondary stream |
| t | throat, primary nozzle |

[redacted]

| | |
|---|---|
| tun | tunnel |
| w | wall |
| 0 | free stream |
| 1 | station 1, sketch (b) |

[redacted]

APPENDIX B

THRUST CALCULATIONS

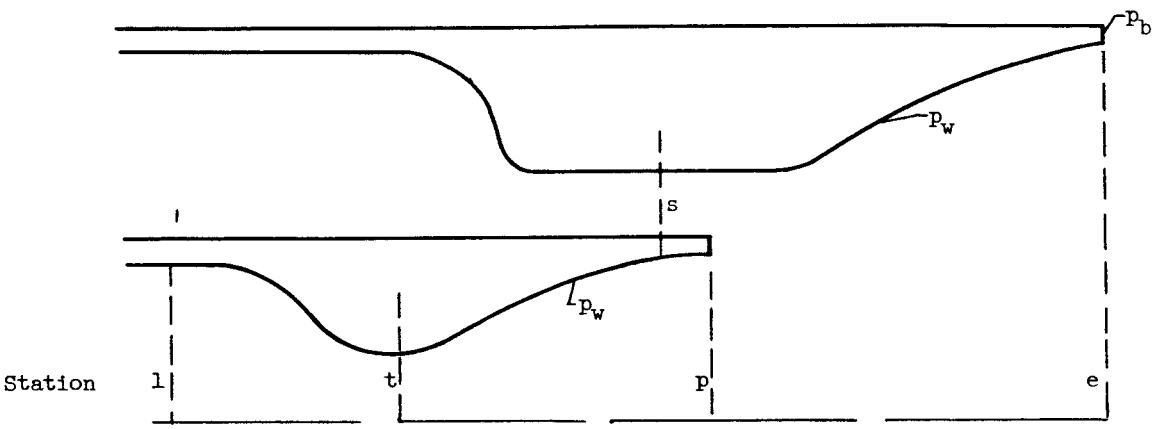


(b)

Exit Momentum

The exit momentum is

$$\mathcal{M}_e = \int^{A_e} (p + \rho v^2) dA$$

From the momentum equation neglecting wall friction, the exit momentum was computed as follows:

$$\mathcal{M}_e = (p_1 + \gamma M_1^2) A_1 + \int_{A_1}^{A_p} p_w \, dA + (p_s + \gamma M_s^2) A_s + \int_{A_s}^{A_e} p_w \, dA$$

where $M_1$ and $M_s$ were computed from measurements of $(p/P)_1$ and $(p/P)_s$.

[redacted]

## Tunnel Thrust

Thrust and ideal thrust are

$$F = \mathcal{M}_e - p_0 A_e$$

and

$$F_{p,id} = m_p v_{e,id}$$

where $m_p$ is the measured primary flow and $v_{e,id}$ is the ideal exit velocity based on the particular value of $P_p/p_0$.

## Calculated Quiescent Thrust

If it is assumed that conditions at the nozzle exit (pressure, velocity, etc.) are determined only by the "effective ambient" pressure $p_b$, then $\mathcal{M}_e$ is a function only of $P_p/p_b$ and $\omega\sqrt{\tau}$. The thrust that would occur under quiescent conditions can be obtained from

$$F = \mathcal{M}_e - p_b A_e$$

and

$$F_{p,id} = m_p v_{e,id}$$

where $v_{e,id}$ is now the velocity based on $P_p/p_b$.

Tunnel measurements at an effective pressure ratio $P_p/p_b$ can then be used to estimate quiescent performance at a pressure ratio

$$(P_p/p_0)_q = (P_p/p_b)_{tun}$$

Because of the order followed in taking data, figures 9 and 10 are cross plots of the data.

## Calculated Flight-Path Thrust

A typical flight path was chosen for a missile with a given chamber pressure $P_p$. The base pressure ratio $p_b/p_0$ was assumed (fig. 11). From this data, $F_{id}$, $P_p/p_b$, and the maximum $P_s/p_p$ obtainable from a

[redacted]

normal-shock inlet were calculated. The range of $\omega\sqrt{\tau}$ possible is determined by $P_s/P_p$ from figure 4. The thrust ratio $F/F_{p,id}$ was found from figure 9 or 10 using $P_p/p_b$ and the $\omega\sqrt{\tau}$ that gave the highest corrected thrust. The corrected thrust was then

$$\frac{F}{F_{p,id}} + \frac{(p_b - p_0)A_e}{F_{p,id}} - \frac{m_s v_0}{F_{p,id}}$$

The convergent-divergent-nozzle thrust ratio was calculated by assuming an ideal fixed nozzle having a design pressure ratio of 89.5. The results were then reduced by 0.02.

## APPENDIX C

## THEORETICAL WEIGHT-FLOW RATIO

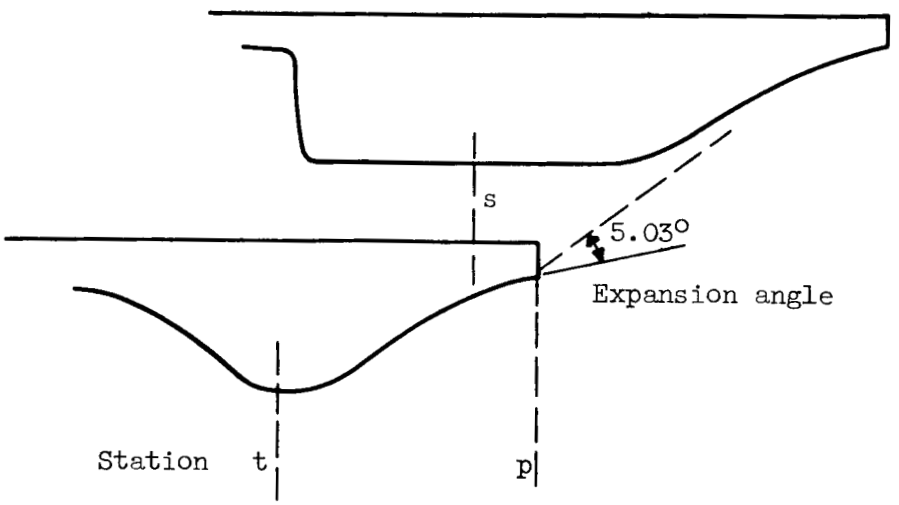


(c)

Assume that the jet pressure ratio $P_p/p_0$ is sufficiently high that, neglecting the effect of secondary flow, the primary stream would expand to the shroud wall.

The weight-flow ratio is then

$$\omega\sqrt{\tau} = \frac{A_s}{A_t}\frac{p_s}{P_p}\frac{(A/A^*)_t}{\left[(A/A^*)(p/P)\right]_s}\frac{\varphi_s}{\varphi_t} \qquad (C1)$$

where $\varphi$ is a flow coefficient.

For low secondary pressures, $A_s$ is not choked, and it can be assumed that $p_s/P_p$ is a function of the shroud angle at the primary-nozzle exit; that is, $p_s/P_p$ is determined by a 5.03° expansion from the primary (see model). Assuming unity flow coefficients, equation (C1) then is

$$\omega\sqrt{\tau} = (A_s/A_t)0.013\frac{1}{\left[(A/A^*)(p/P)\right]_s} \qquad (C1a)$$

[redacted]

and the ejector pressure ratio is

$$P_s/P_p = 0.013(P/p)_s \qquad (C2)$$

Both weight flow and ejector pressure ratio can then be obtained as a function of secondary Mach number $M_s$.

For high secondary pressures $\left(P_s/P_p > \frac{0.0130}{0.528} = 0.0245\right)$, $A_s$ can be choked; and, again assuming unity flow coefficients,

$$\omega\sqrt{\tau} = (A_s/A_t)(P_s/P_p) \qquad (C1b)$$

The theoretical curves of figure 4 were obtained from equations (C1a), (C1b), and (C2).



## REFERENCES

1. Beheim, Milton A.: Off-Design Performance of Divergent Ejectors. NACA RM E58G10a, 1958.

2. Greathouse, William K., and Beale, William T.: Performance Characteristics of Several Divergent-Shroud Aircraft Ejectors. NACA RM E55G21a, 1955.

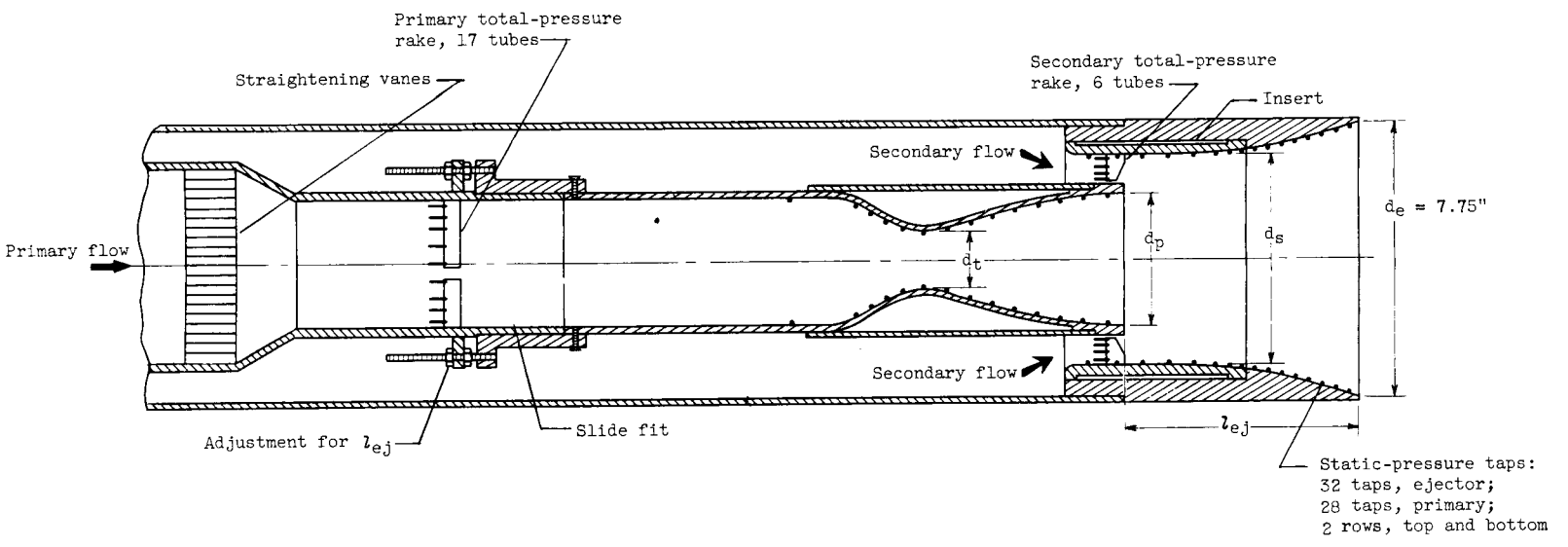


Figure 1. - Cross section of model.

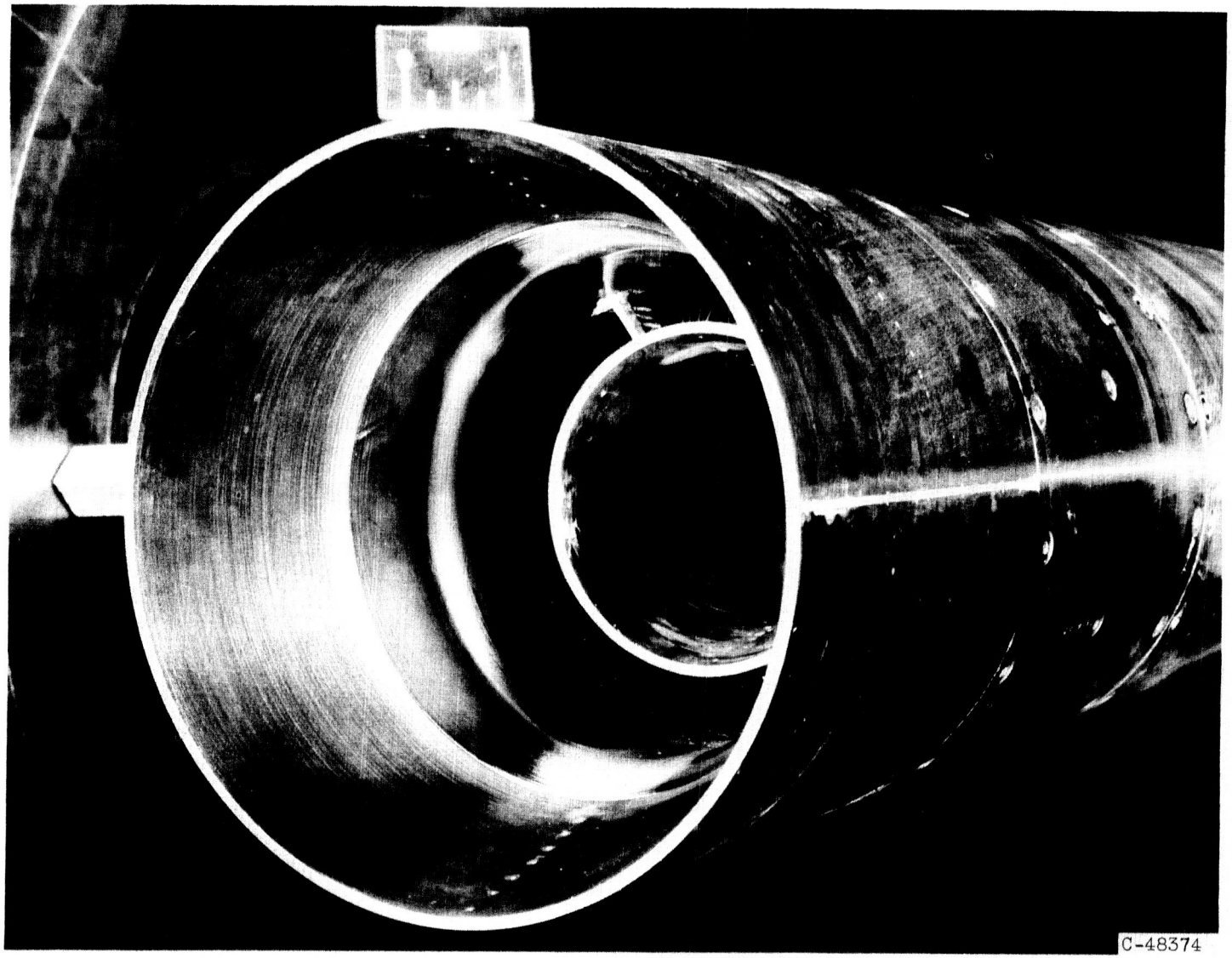


Figure 2. - Photograph of model.

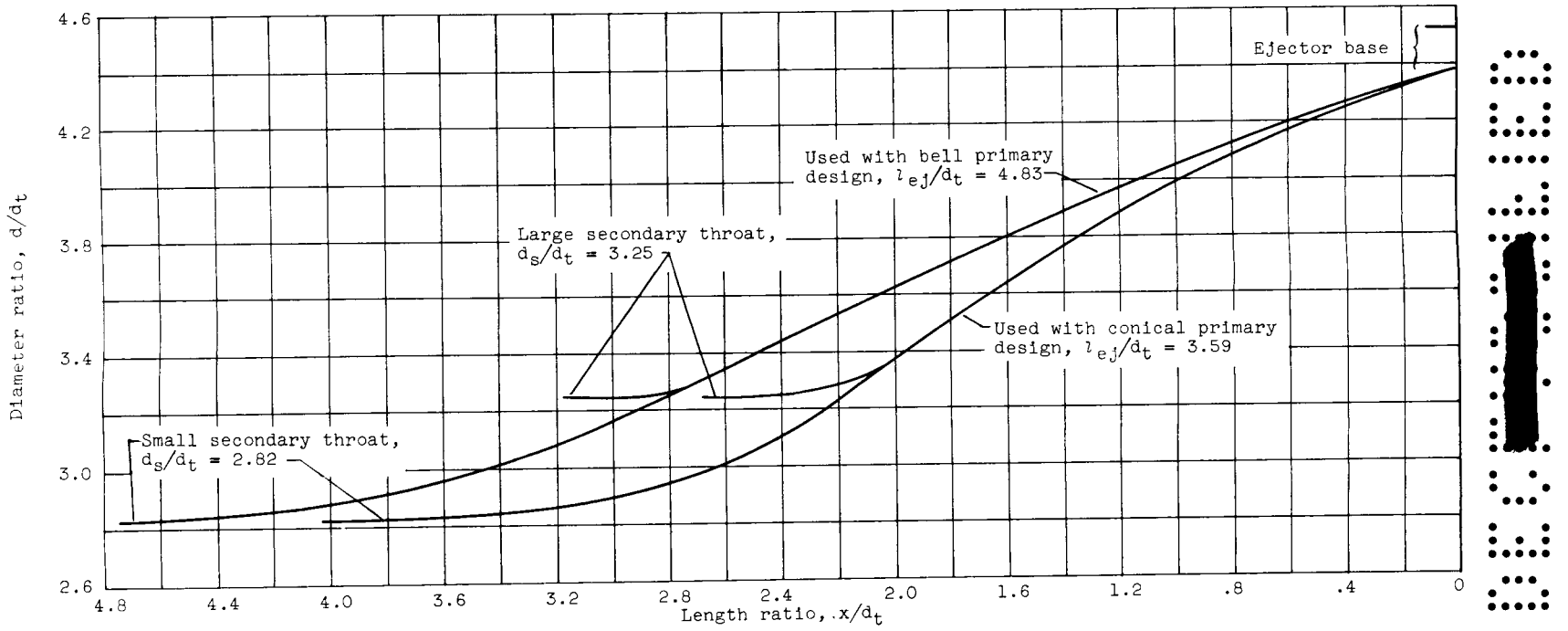


(a) Ejector contours.

Figure 3. - Nozzle and ejector contours.

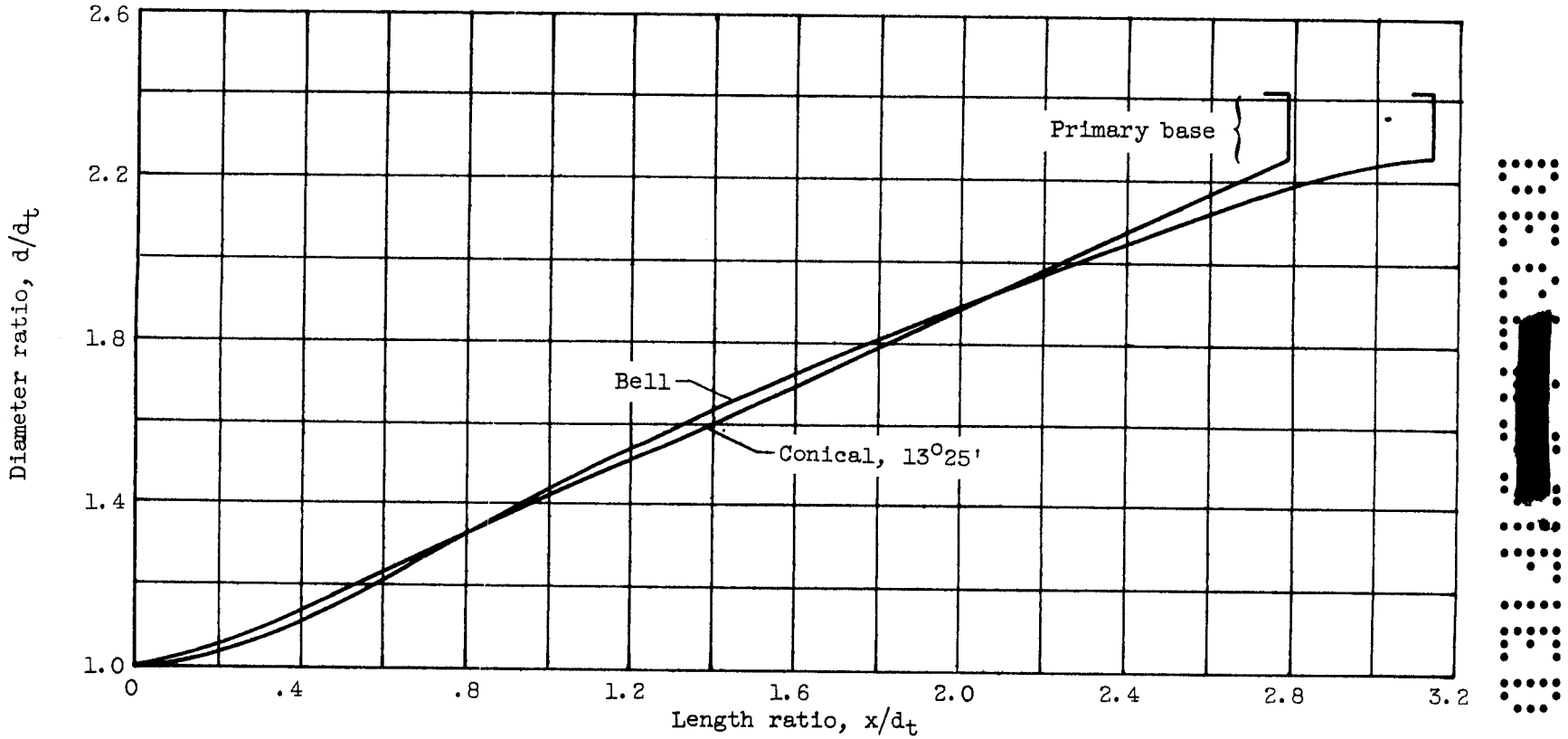


(b) Primary-nozzle contours.

Figure 3. - Concluded. Nozzle and ejector contours.

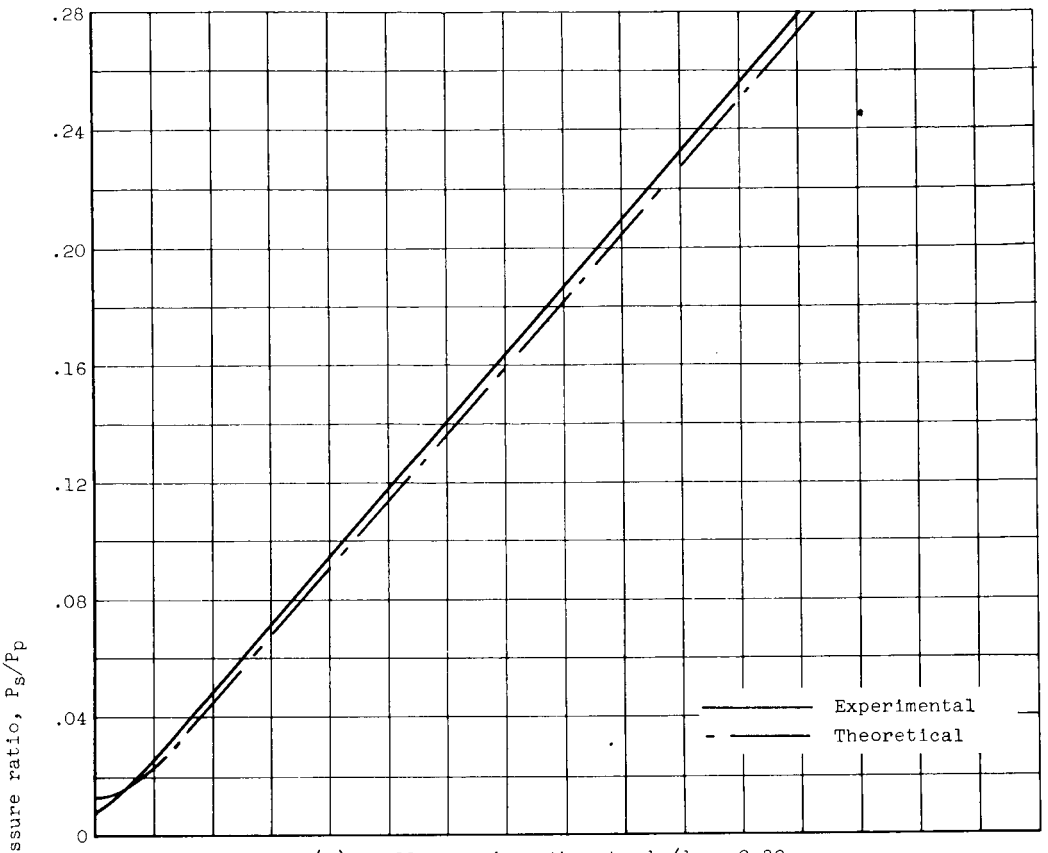


(a) Small secondary throat; $d_s/d_t = 2.82$.

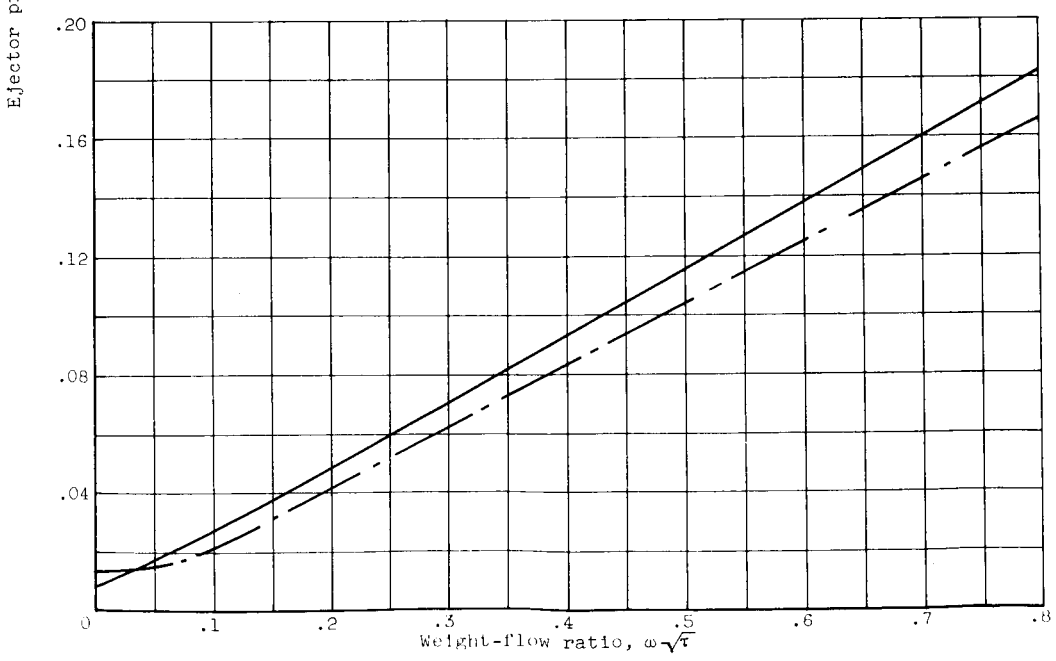


(b) Large secondary throat; $d_s/d_t = 3.25$.

Figure 4. - Ejector pumping characteristics.

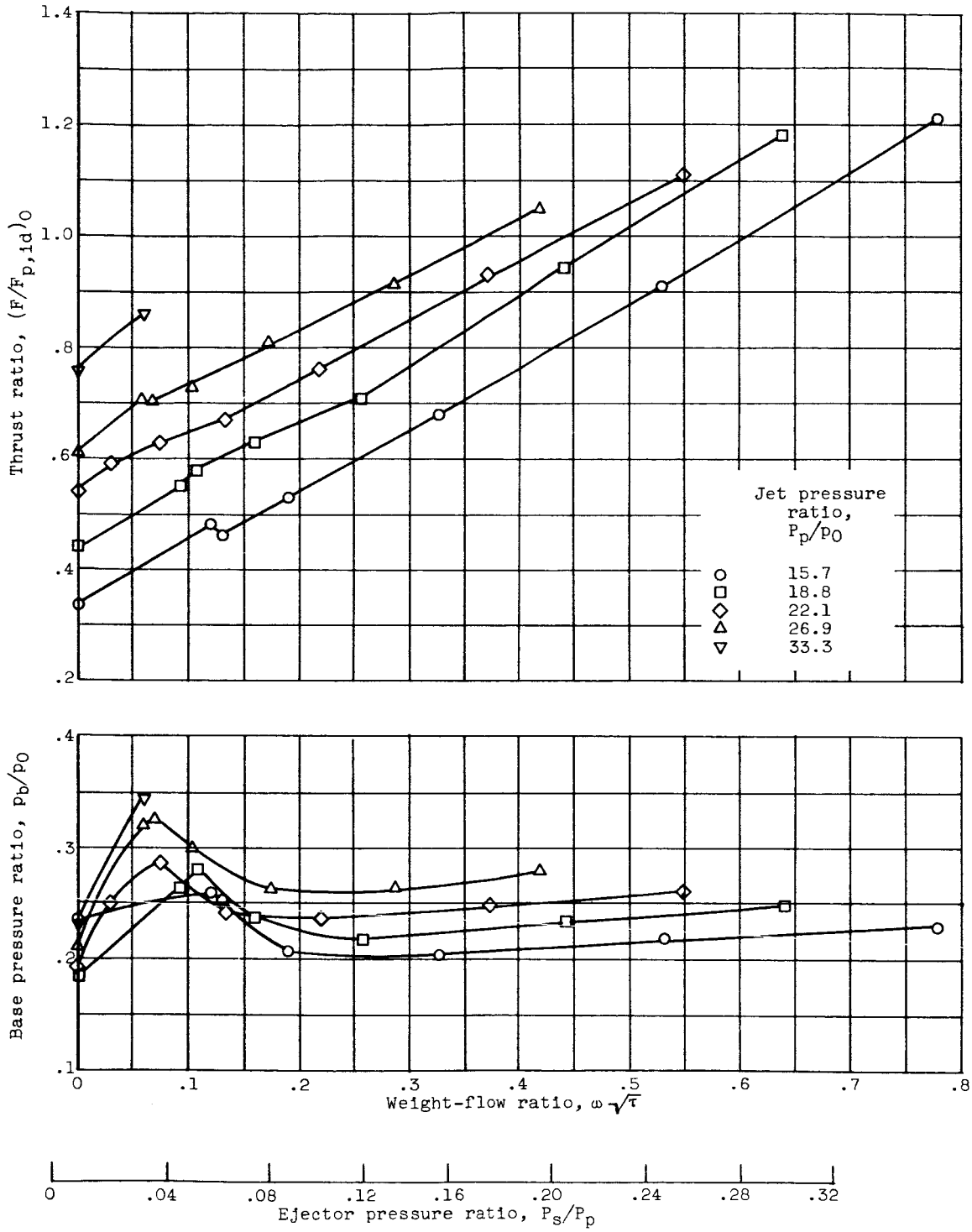


(1) Length-diameter ratio, $l_{ej}/d_t$, 3.59 (design).

(a) Ejector diameter ratio, $d_s/d_t$, 2.82.

Figure 5. - Performance of ejector with conical primary nozzle.

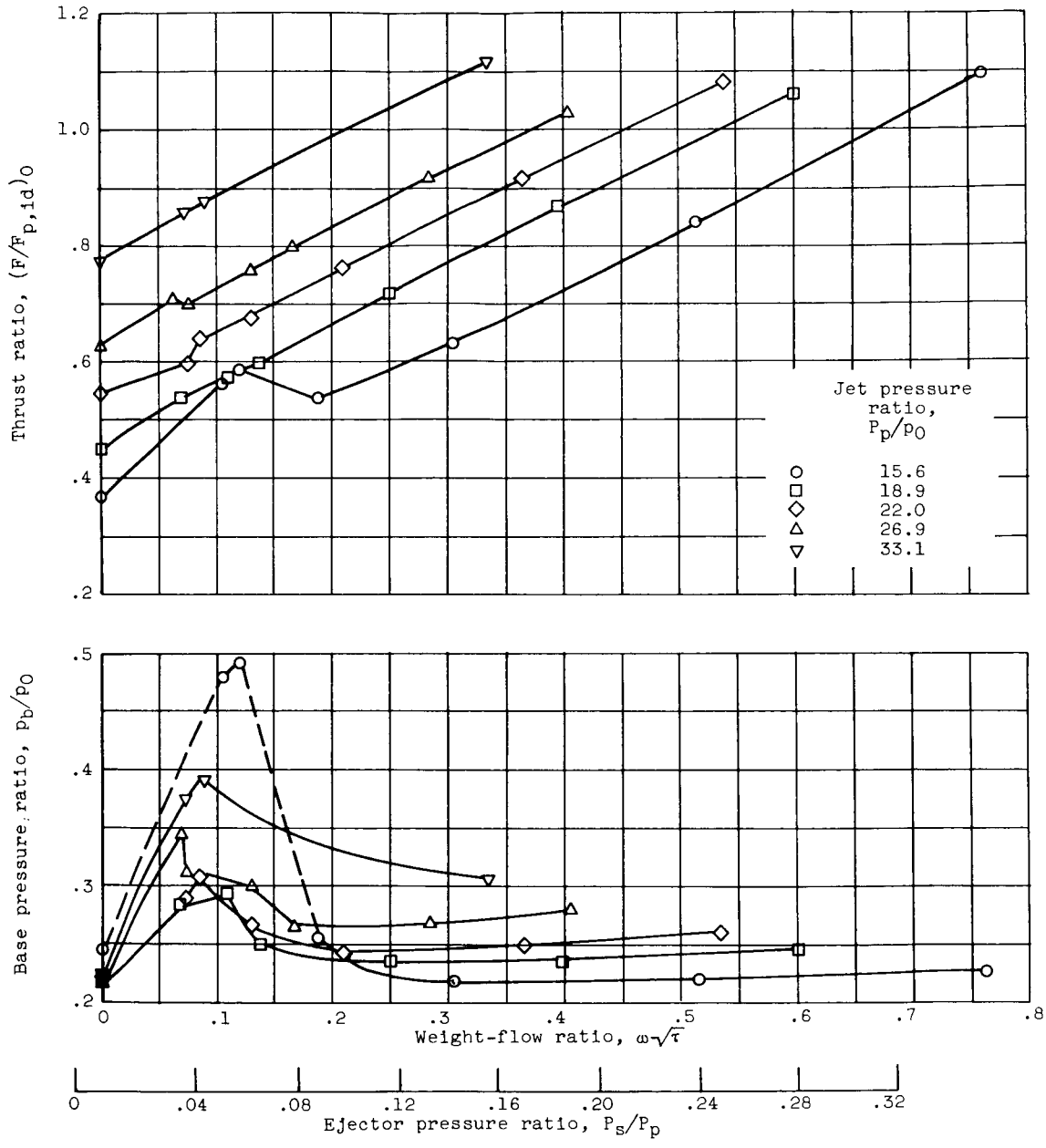


(2) Length-diameter ratio, $l_{ej}/d_t$, 3.45.

(a) Continued. Ejector diameter ratio, $d_s/d_t$, 2.82.

Figure 5. - Continued. Performance of ejector with conical primary nozzle.

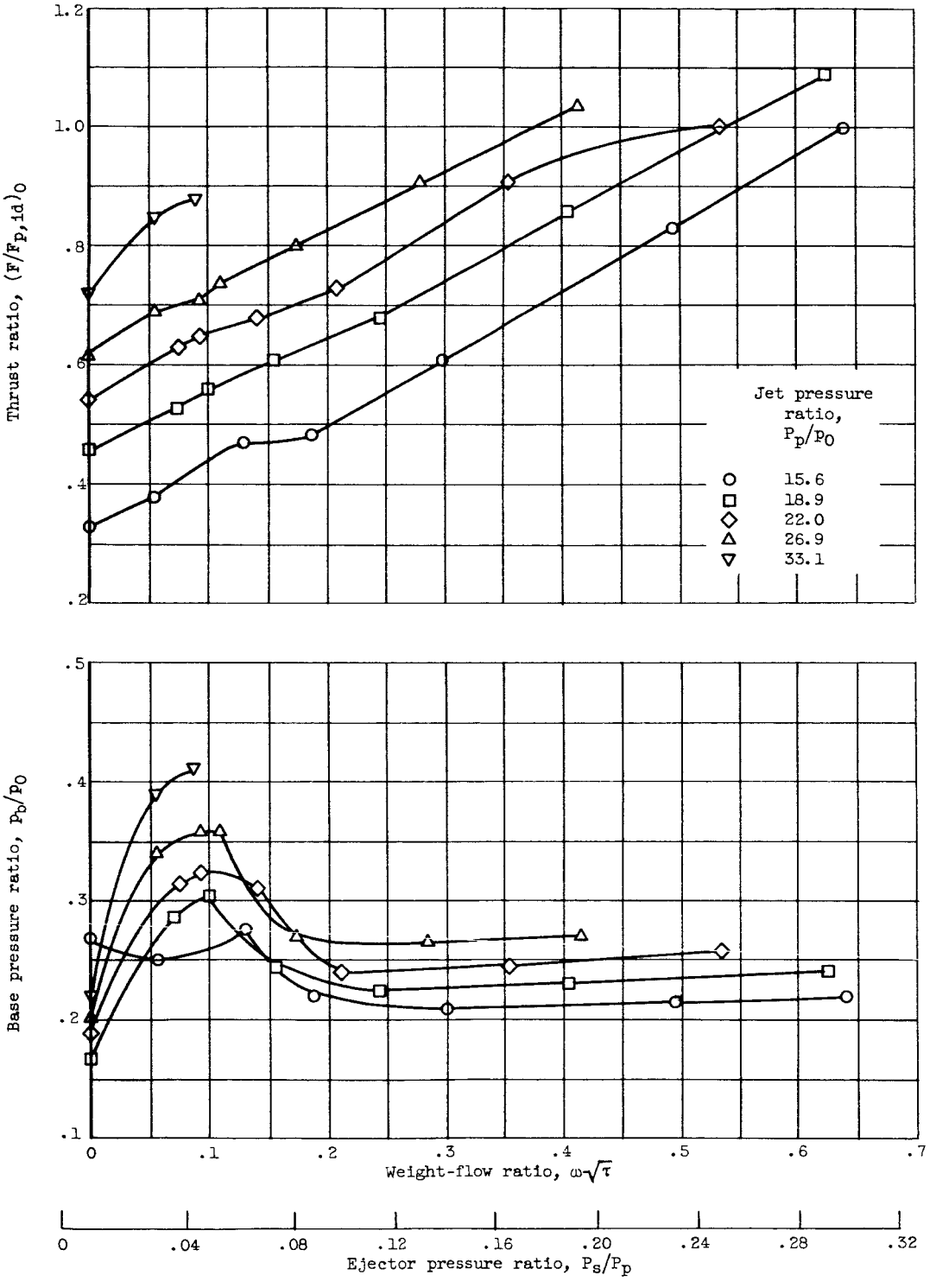


(3) Length-diameter ratio, $l_{ej}/d_t$, 3.31.

(a) Continued. Ejector diameter ratio, $d_s/d_t$, 2.82.

Figure 5. - Continued. Performance of ejector with conical primary nozzle.

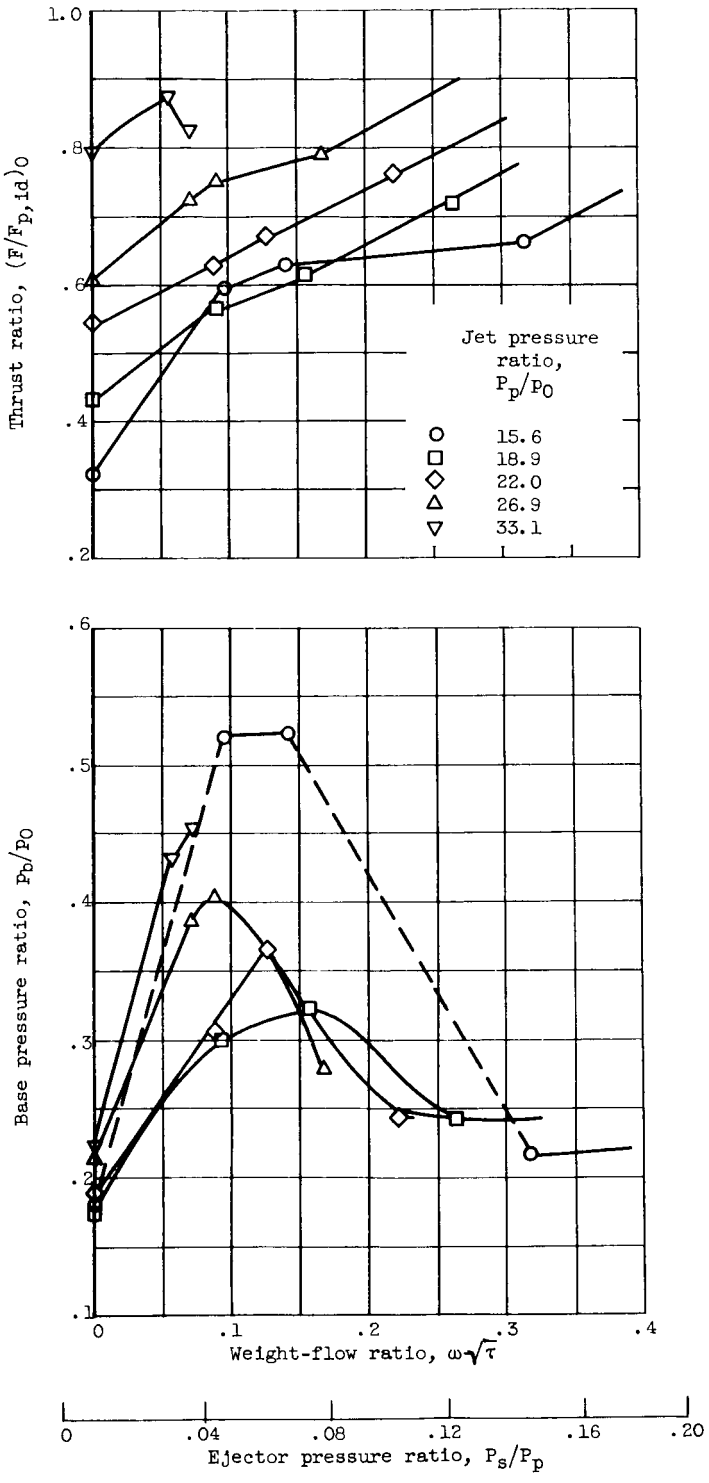


(4) Length-diameter ratio, $l_{ej}/d_t$, 2.74.

(a) Concluded. Ejector diameter ratio, $d_s/d_t$, 2.82.

Figure 5. - Continued. Performance of ejector with conical primary nozzle.

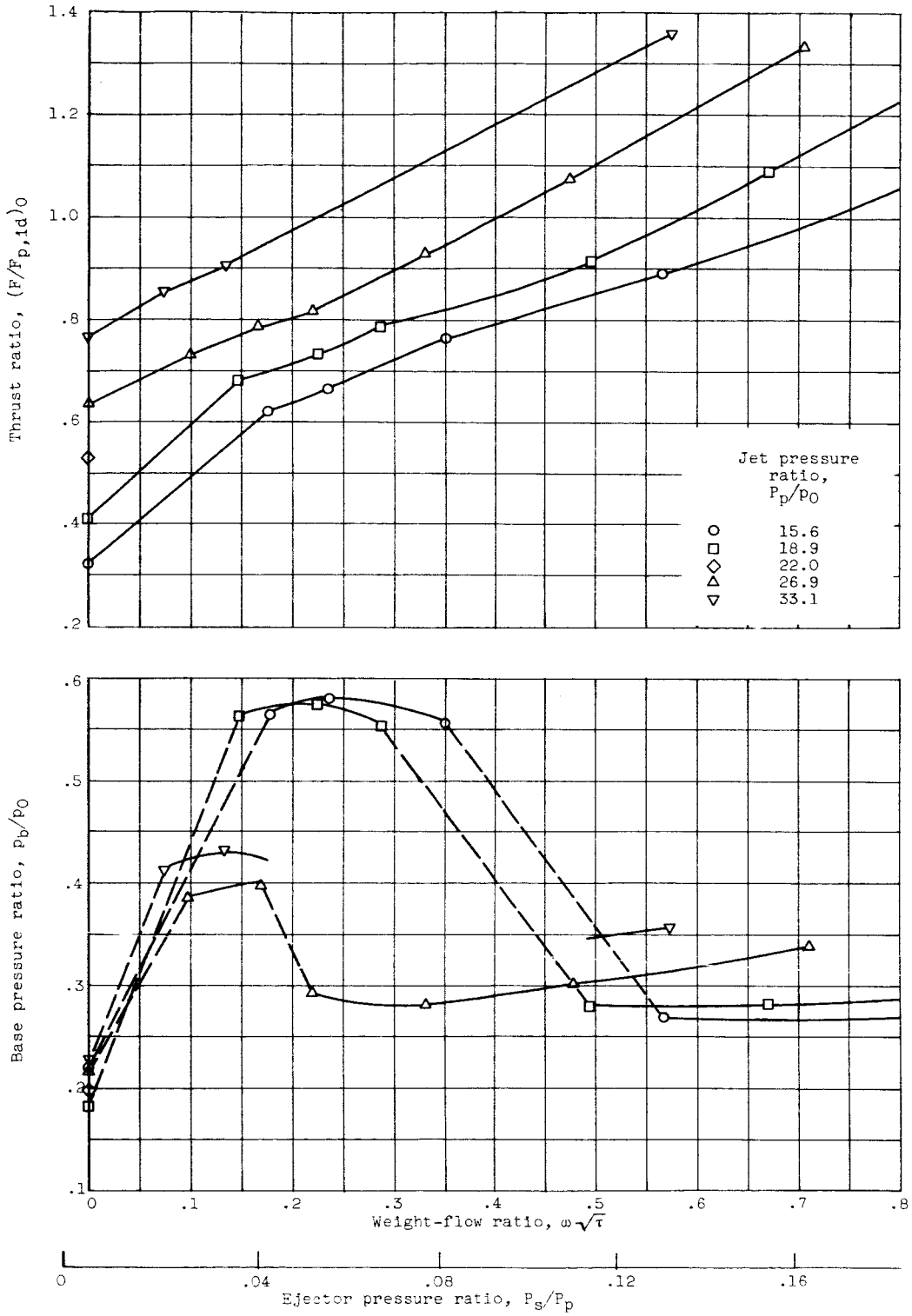


(a) Length-diameter ratio, $l_{ej}/d_t$, 3.59 (design).

(b) Ejector diameter ratio, $d_s/d_t$, 3.25.

Figure 5. - Continued. Performance of ejector with conical primary nozzle.

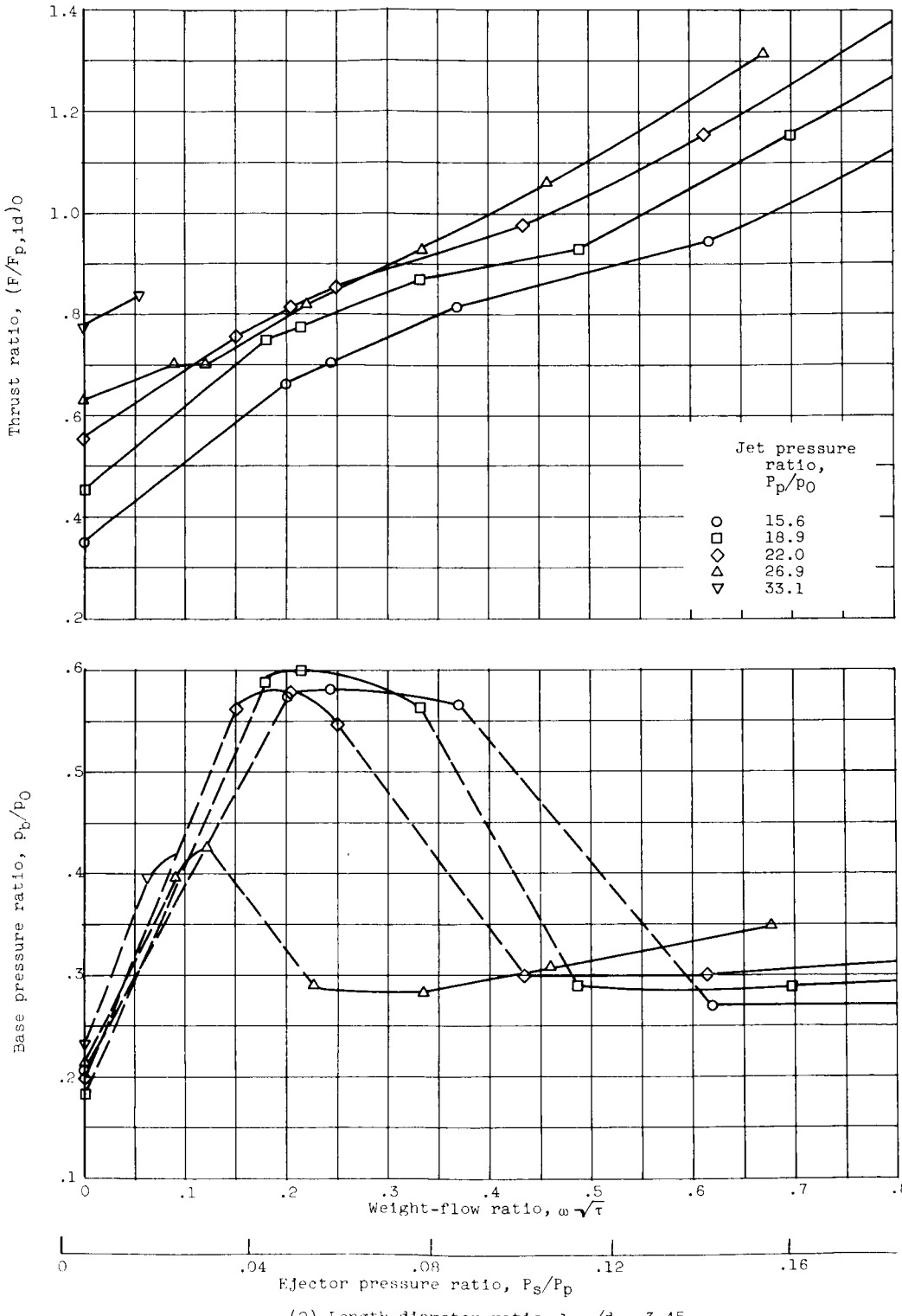


(2) Length-diameter ratio, $l_{ej}/d_t$, 3.45.

(b) Continued. Ejector diameter ratio, $d_s/d_t$, 3.25.

Figure 5. - Continued. Performance of ejector with conical primary nozzle.

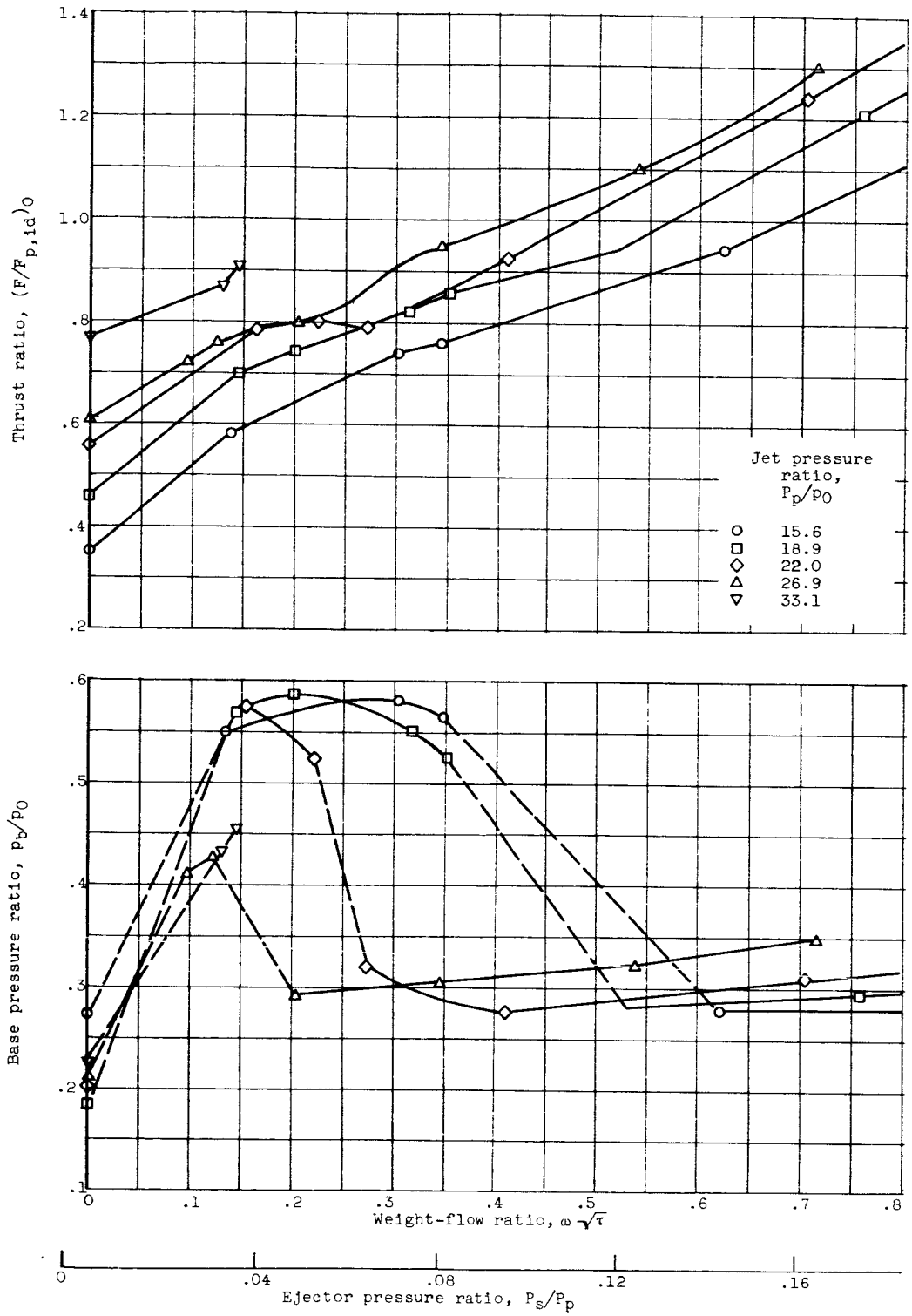


(3) Length-diameter ratio, $l_{ej}/d_t$, 3.31.

(b) Concluded. Ejector diameter ratio, $d_s/d_t$, 3.25.

Figure 5. - Concluded. Performance of ejector with conical primary nozzle.

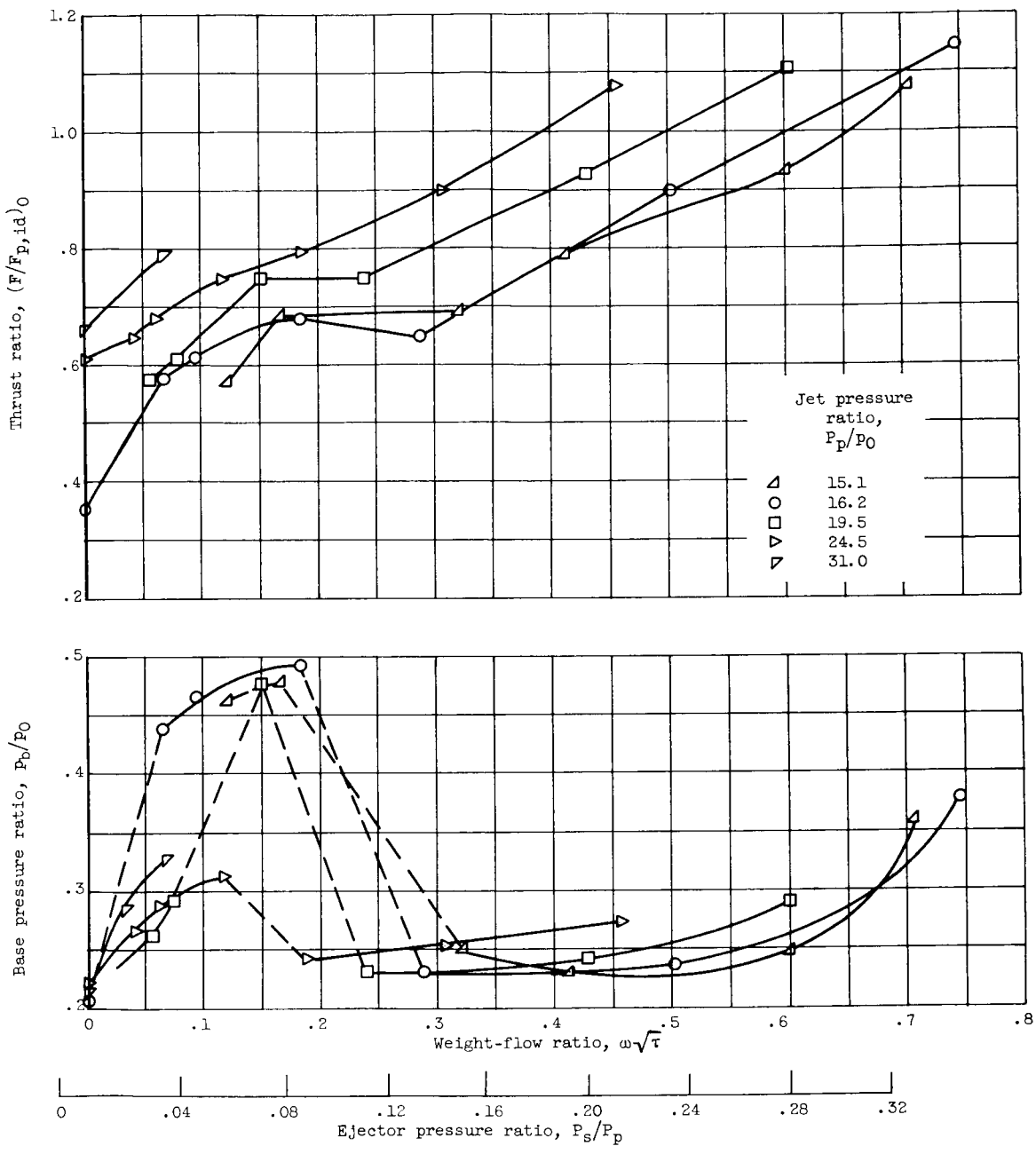


(1) Length-diameter ratio, $l_{ej}/d_t$, 4.83 (design).

(a) Ejector diameter ratio, $d_s/d_t$, 2.82.

Figure 6. - Performance of ejector with bell primary nozzle.

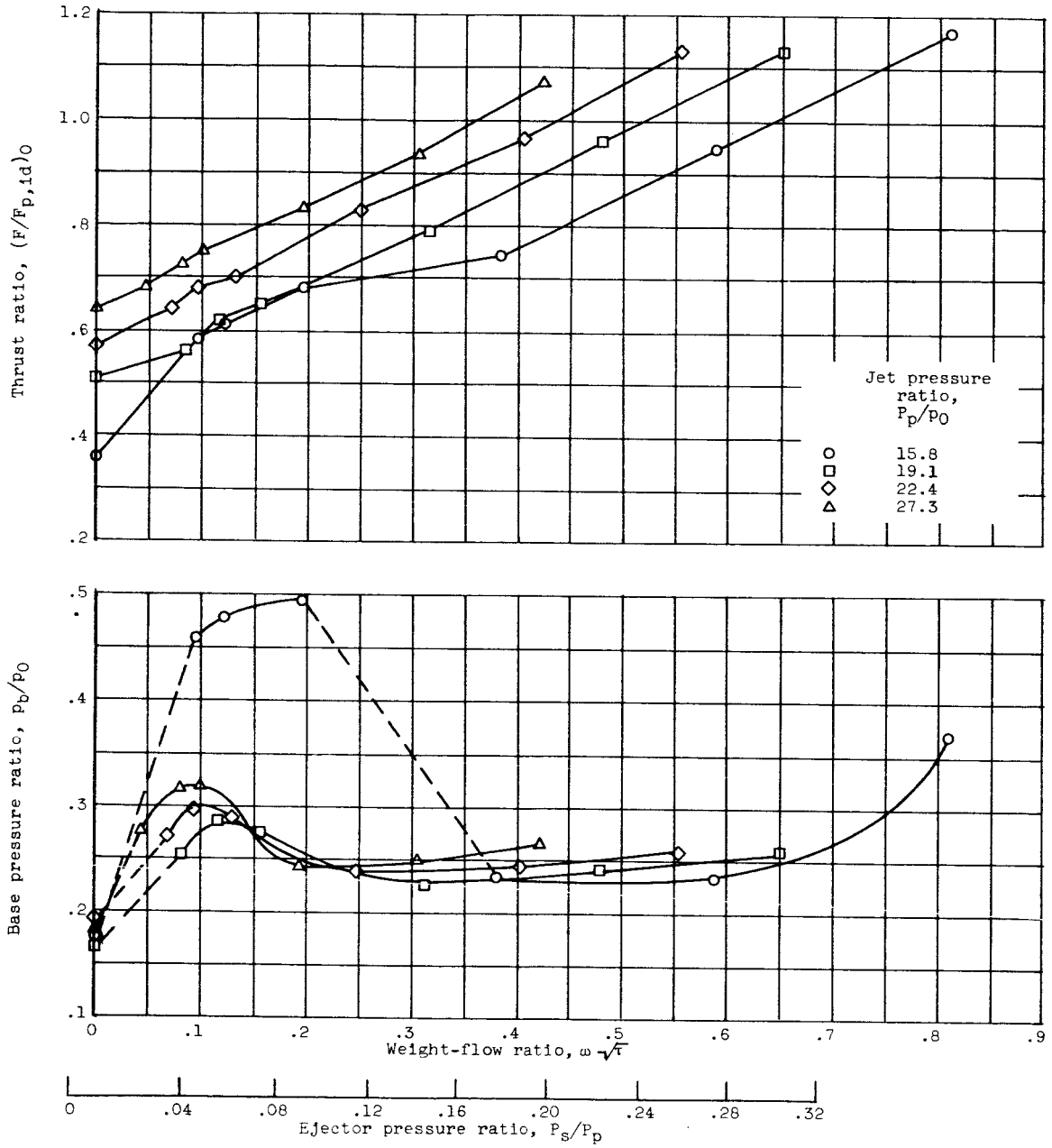


(2) Length-diameter ratio, $l_{ej}/d_t$, 4.68.

(a) Continued. Ejector diameter ratio, $d_s/d_t$, 2.82.

Figure 6. - Continued. Performance of ejector with bell primary nozzle.

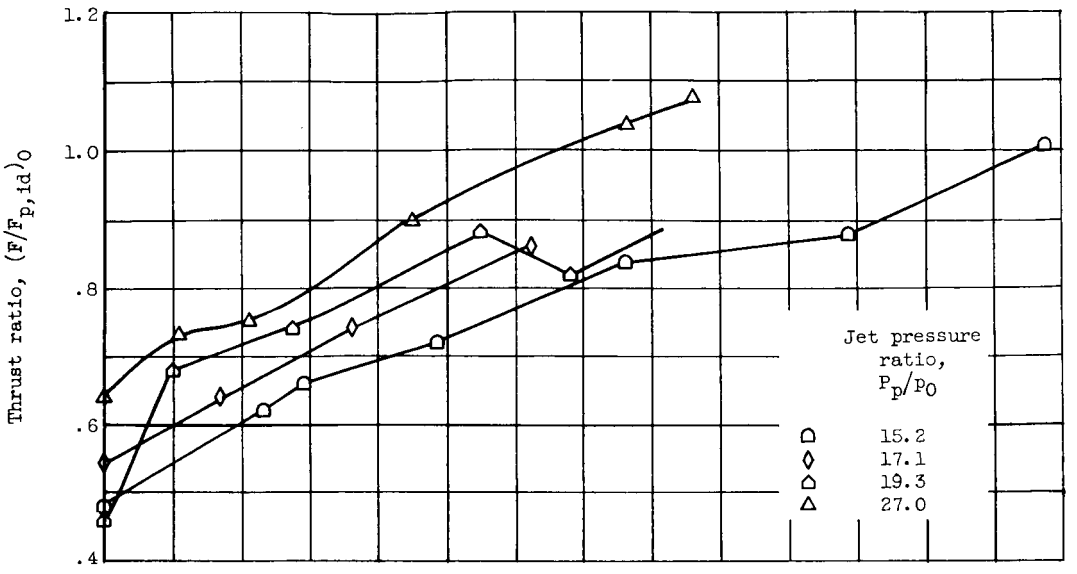


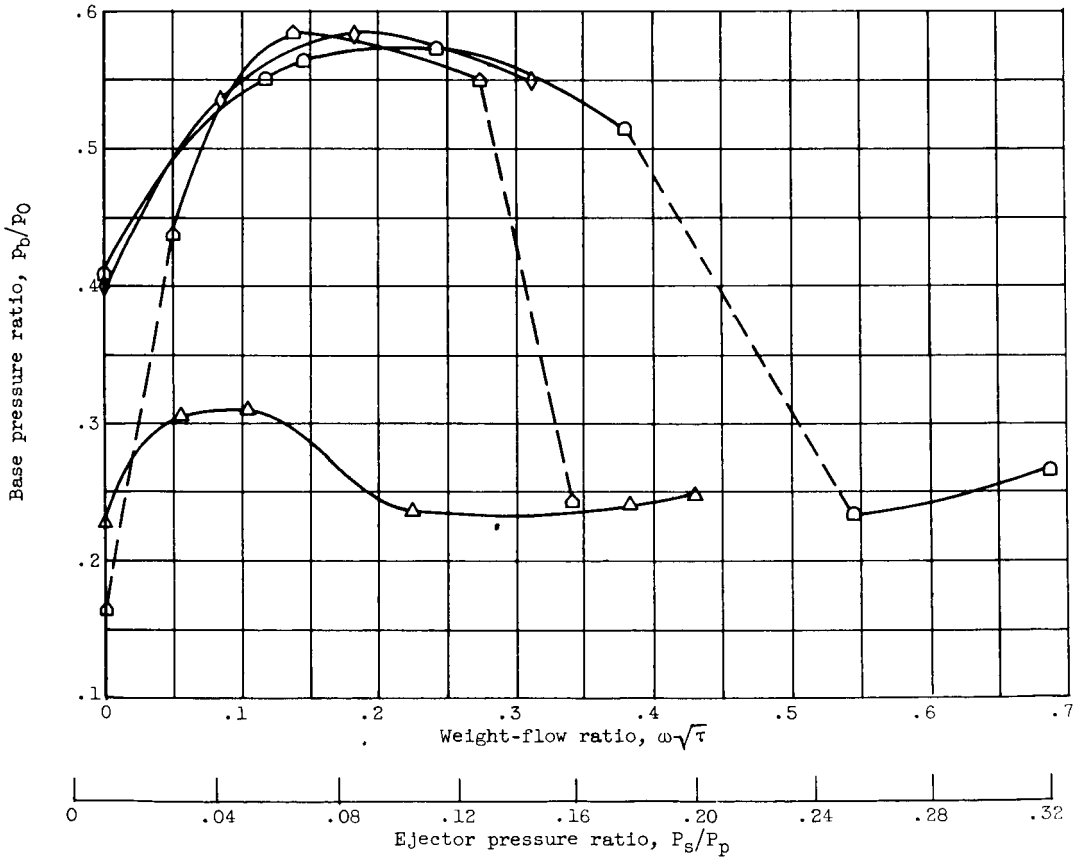


(3) Length-diameter ratio, $l_{ej}/d_t$, 4.55.

(a) Continued. Ejector diameter ratio, $d_s/d_t$, 2.82.

Figure 6. - Continued. Performance of ejector with bell primary nozzle.

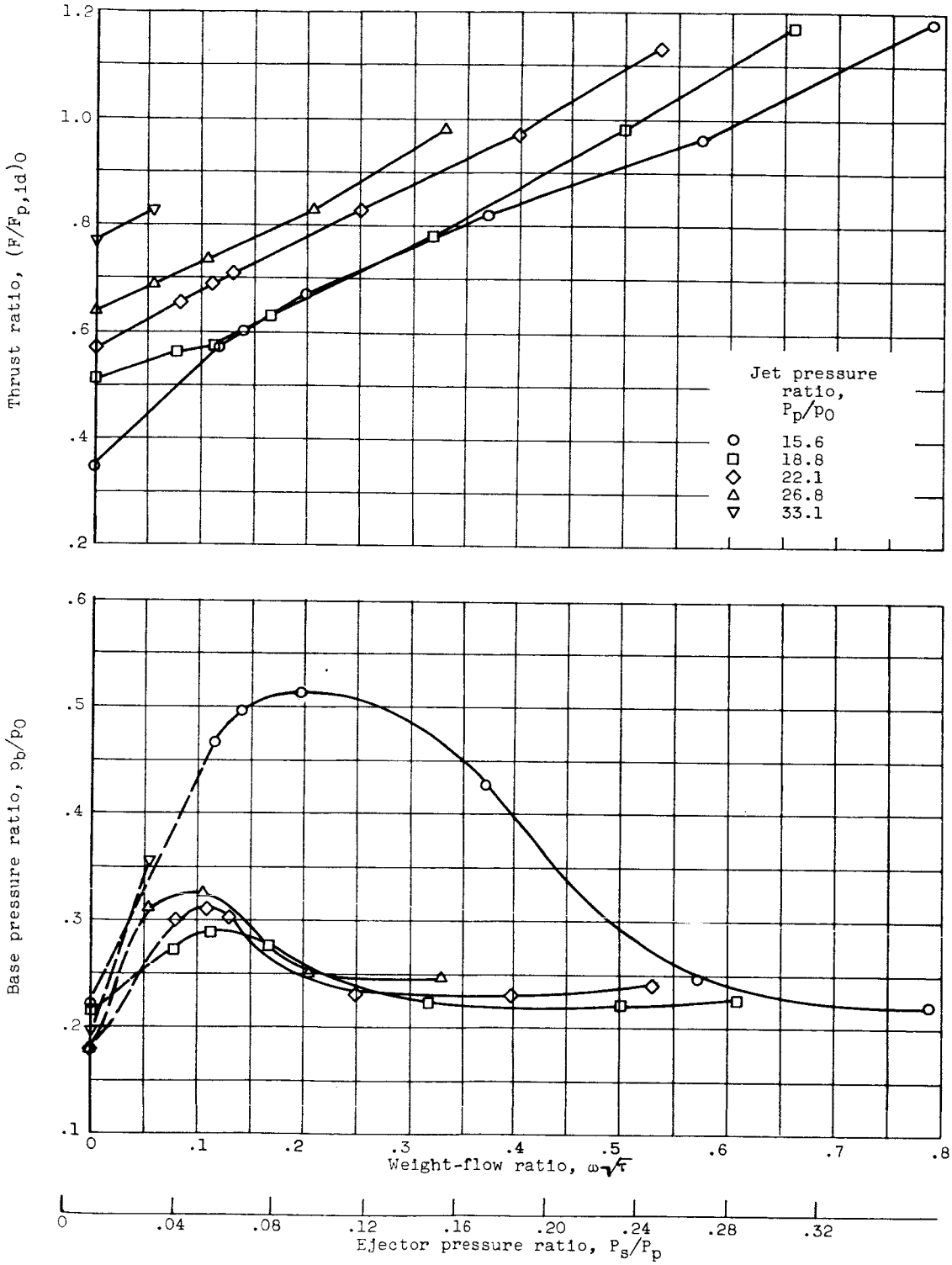


(4) Length-diameter ratio, $l_{ej}/d_t$, 4.26.

(a) Continued. Ejector diameter ratio, $d_s/d_t$, 2.82.

Figure 6. - Continued. Performance of ejector with bell primary nozzle.

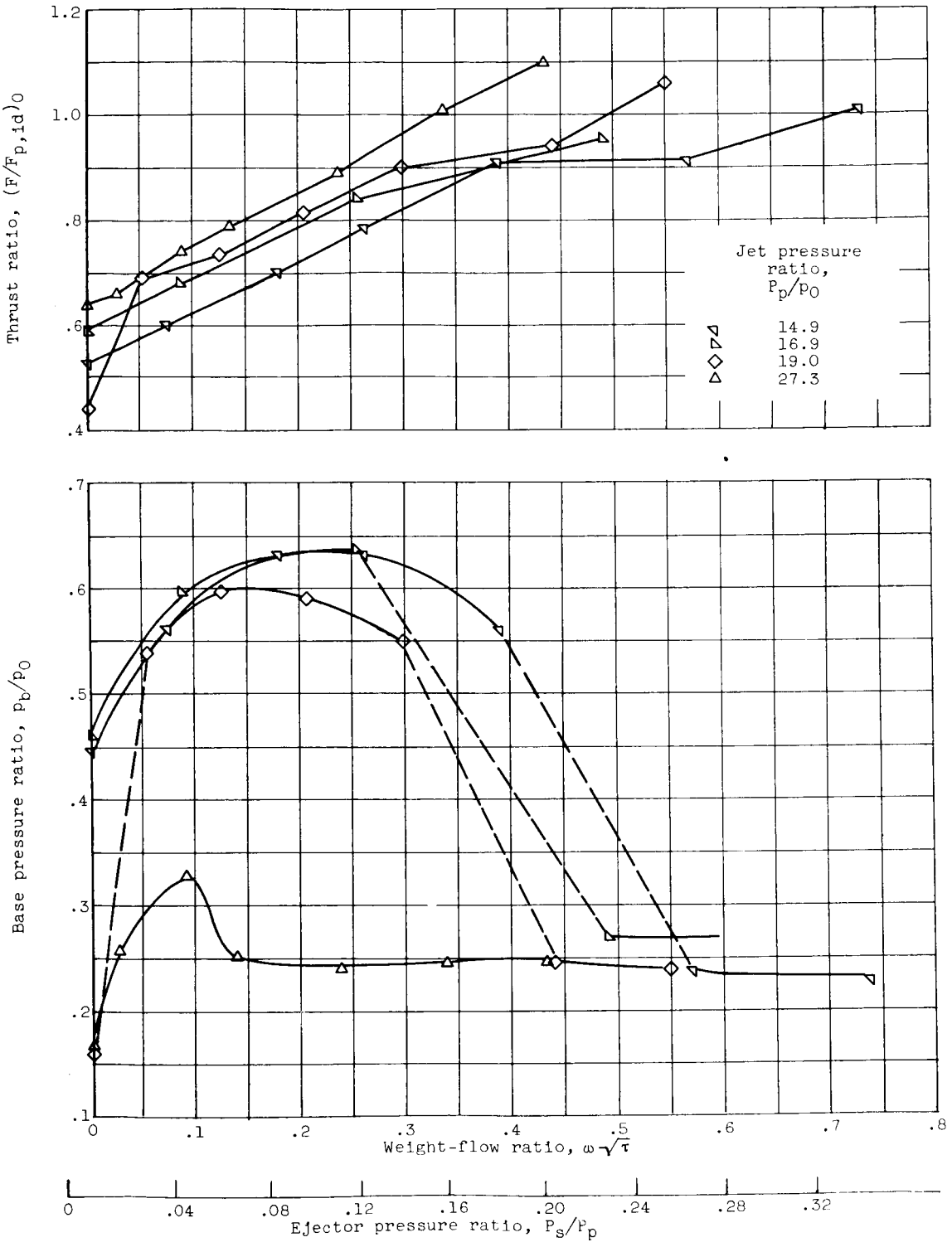


(5) Length-diameter ratio, $l_{ej}/d_t$, 3.98.

(a) Concluded. Ejector diameter ratio, $d_s/d_t$, 2.82.

Figure 6. - Continued. Performance of ejector with bell primary nozzle.

[redacted]

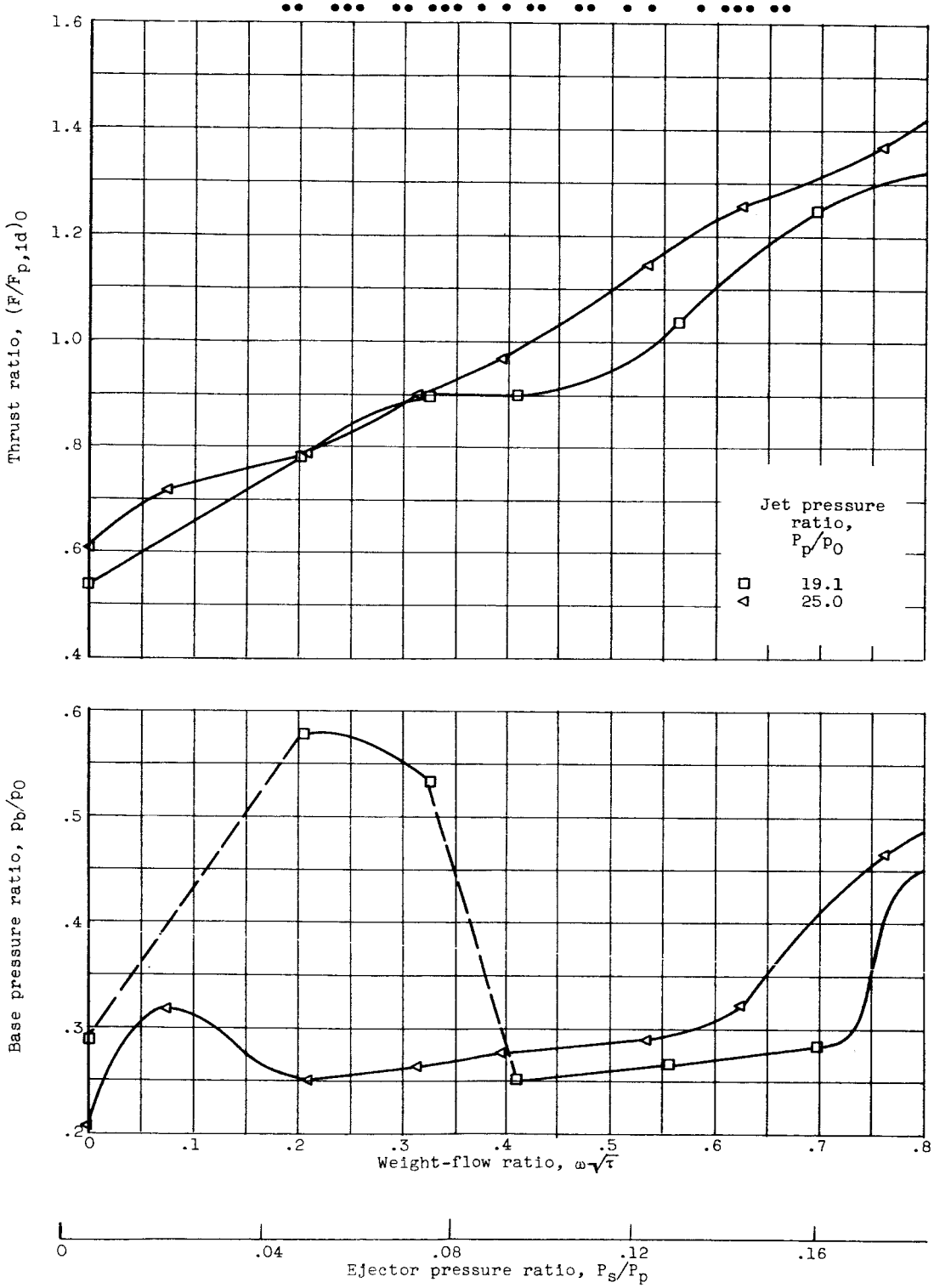


(l) Length-diameter ratio, $l_{ej}/d_t$, 4.83 (design).

(b) Ejector diameter ratio, $d_s/d_t$, 3.25.

Figure 6. - Continued. Performance of ejector with bell primary nozzle.

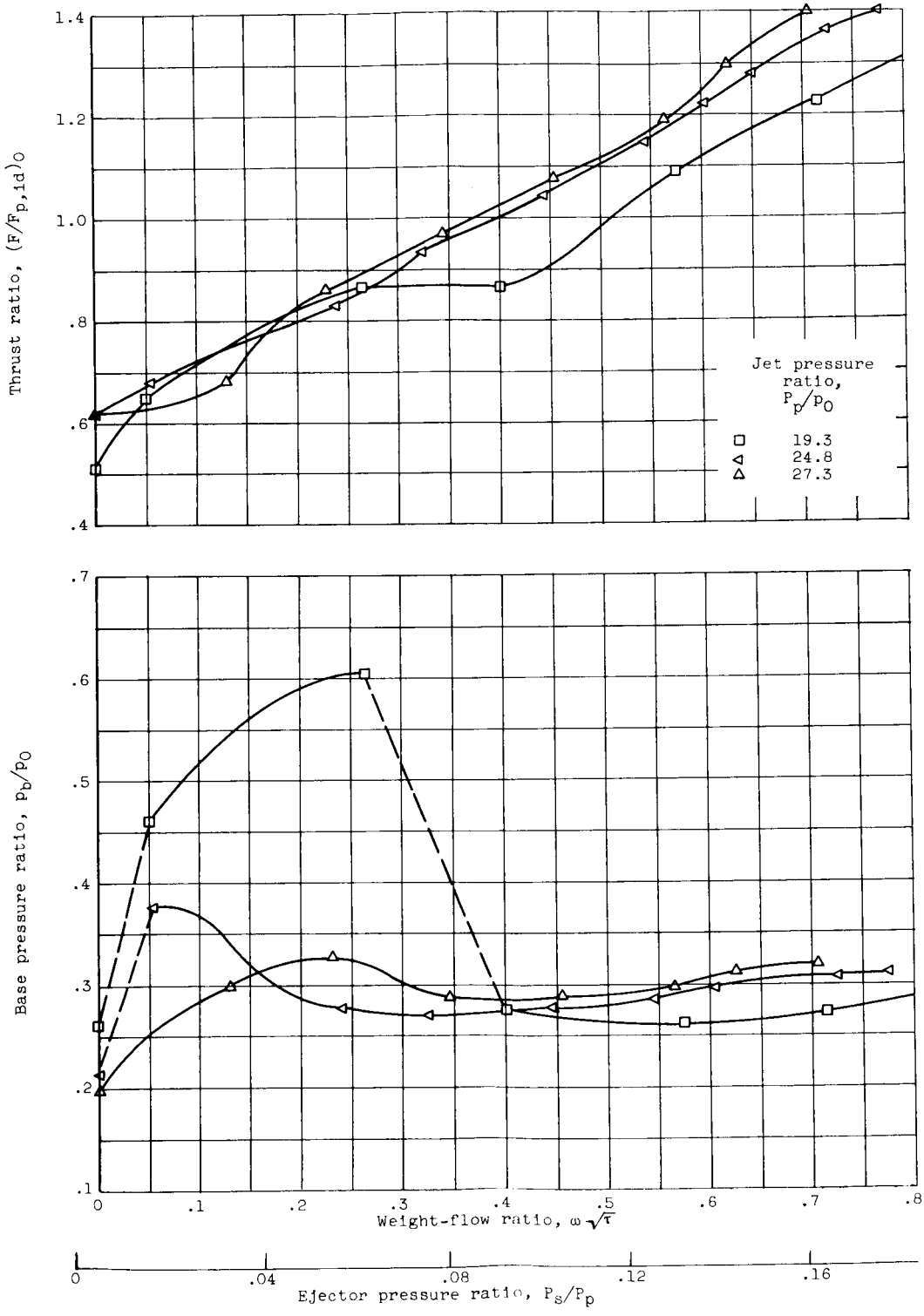


(2) Length-diameter ratio, $l_{ej}/d_t$, 3.98.

(b) Concluded. Ejector diameter ratio, $d_s/d_t$, 3.25.

Figure 6. - Concluded. Performance of ejector with bell primary nozzle.

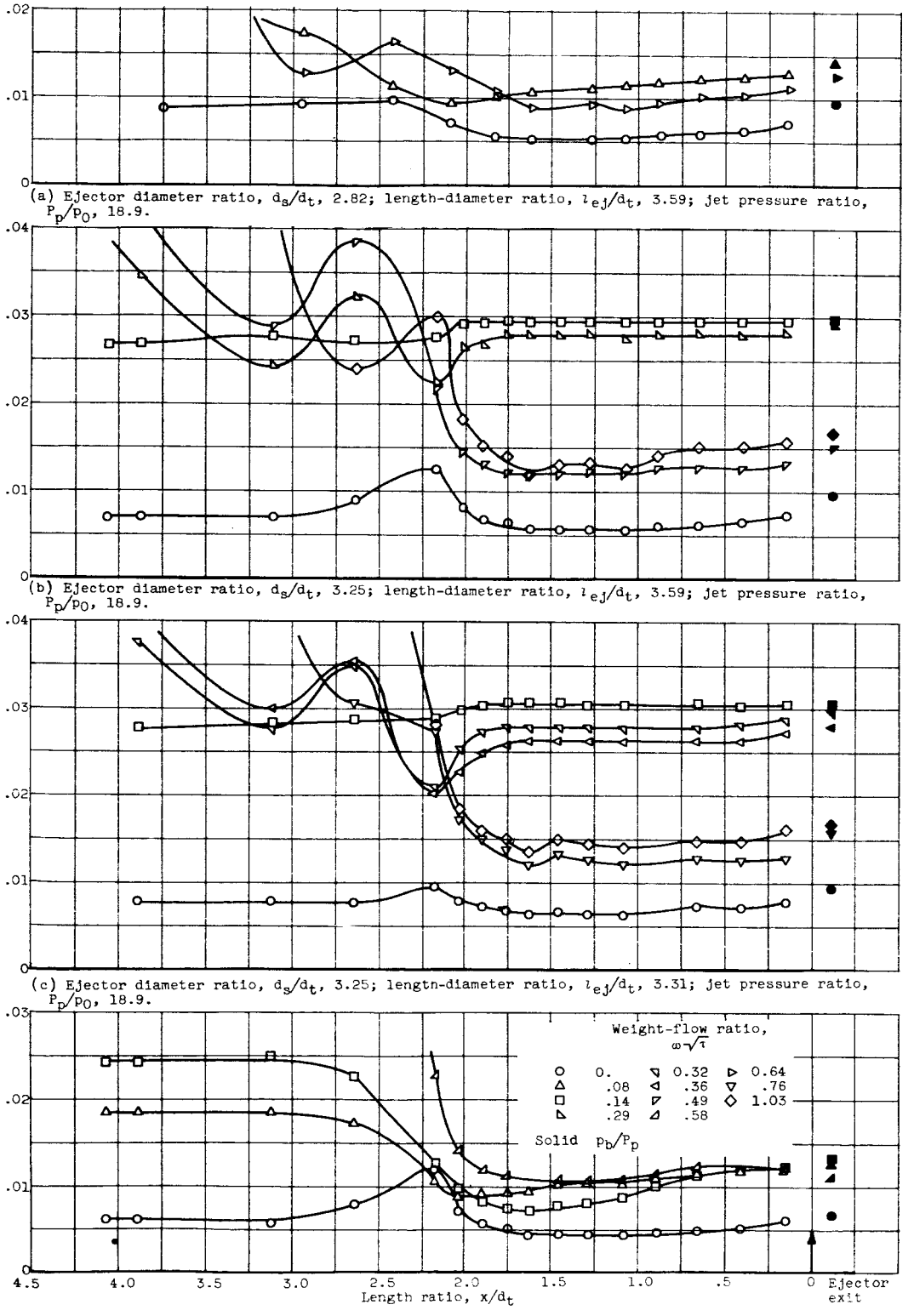


(a) Ejector diameter ratio, $d_s/d_t$, 2.82; length-diameter ratio, $l_{ej}/d_t$, 3.59; jet pressure ratio, $P_p/p_0$, 18.9.

(b) Ejector diameter ratio, $d_s/d_t$, 3.25; length-diameter ratio, $l_{ej}/d_t$, 3.59; jet pressure ratio, $P_p/p_0$, 18.9.

(c) Ejector diameter ratio, $d_s/d_t$, 3.25; lengtn-diameter ratio, $l_{ej}/d_t$, 3.31; jet pressure ratio, $P_p/p_0$, 18.9.

(d) Ejector diameter ratio, $d_s/d_t$, 3.25; length-diameter ratio, $l_{ej}/d_t$, 3.59; jet pressure ratio, $P_p/p_0$, 31.1.

Figure 7. - Ejector wall pressure distributions with the conical primary nozzle.

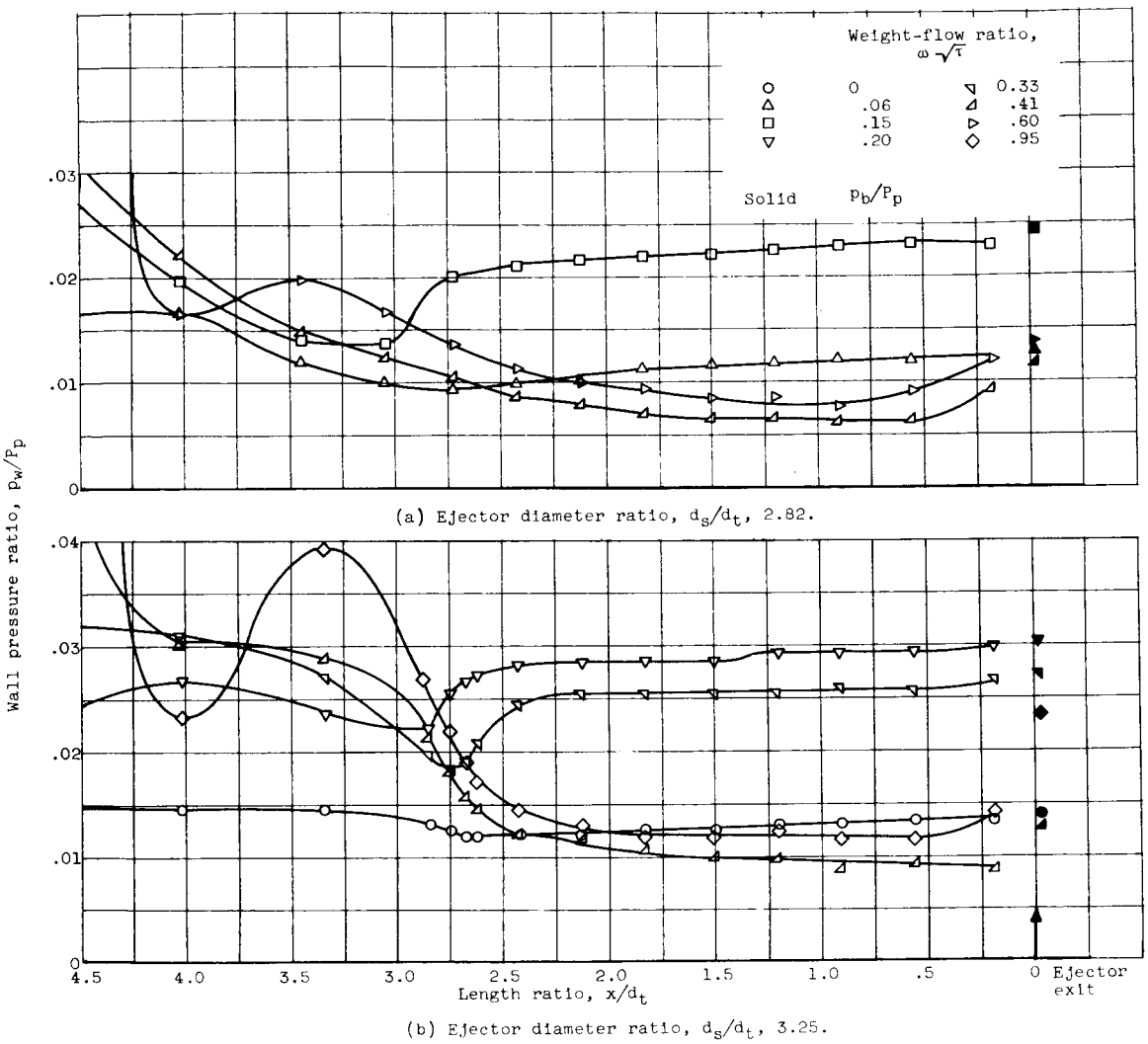


(a) Ejector diameter ratio, $d_s/d_t$, 2.82.

(b) Ejector diameter ratio, $d_s/d_t$, 3.25.

Figure 8. - Ejector wall pressure distributions with bell primary nozzle. Length-diameter ratio, $l_{e,j}/d_t$, 4.83 (design); jet pressure ratio, $P_p/p_0$, 18.9.

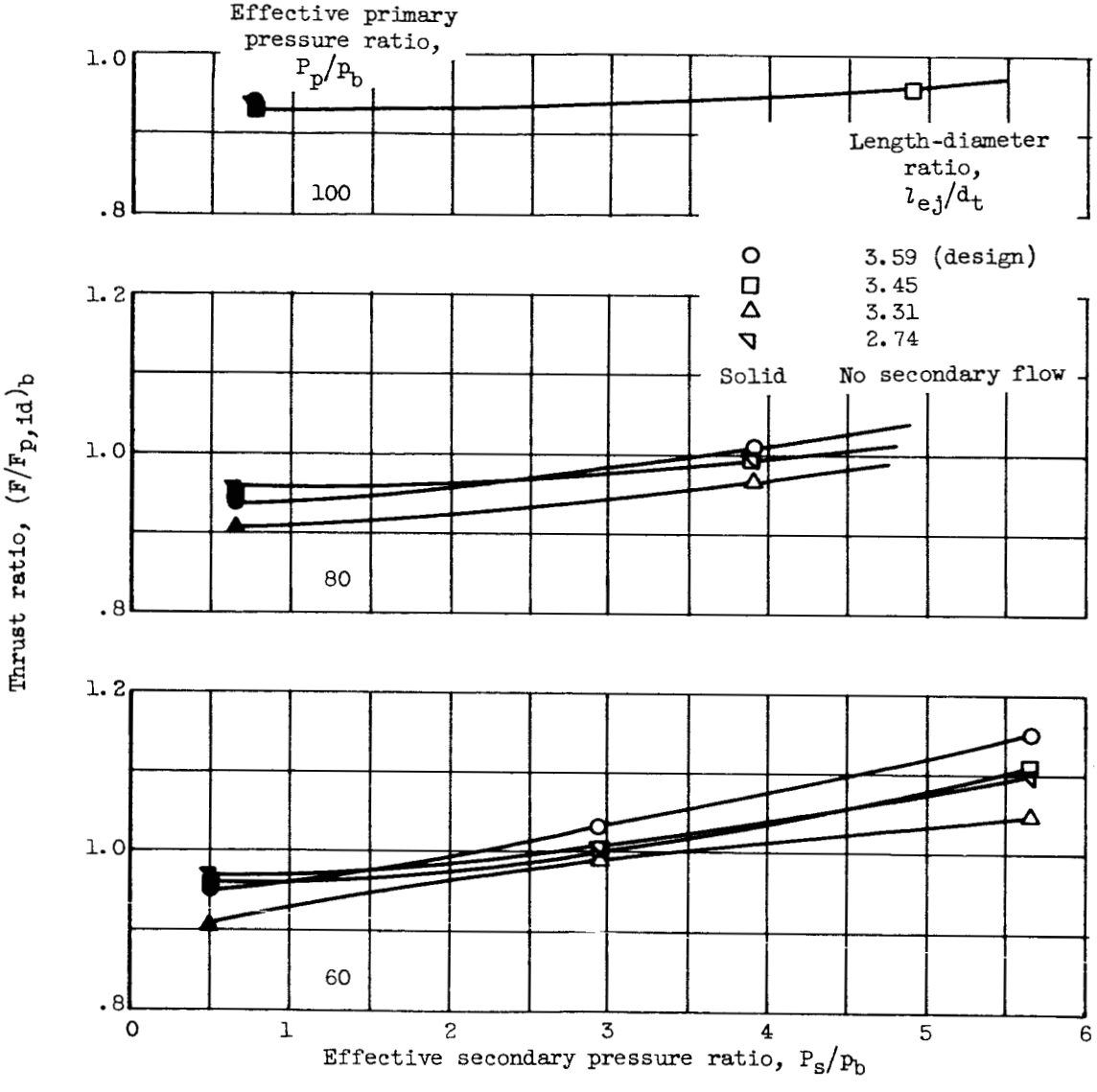


(a) Ejector diameter ratio, $d_s/d_t$, 2.82.

Figure 9. - Calculated performance of ejector with conical primary nozzle in quiescent air.

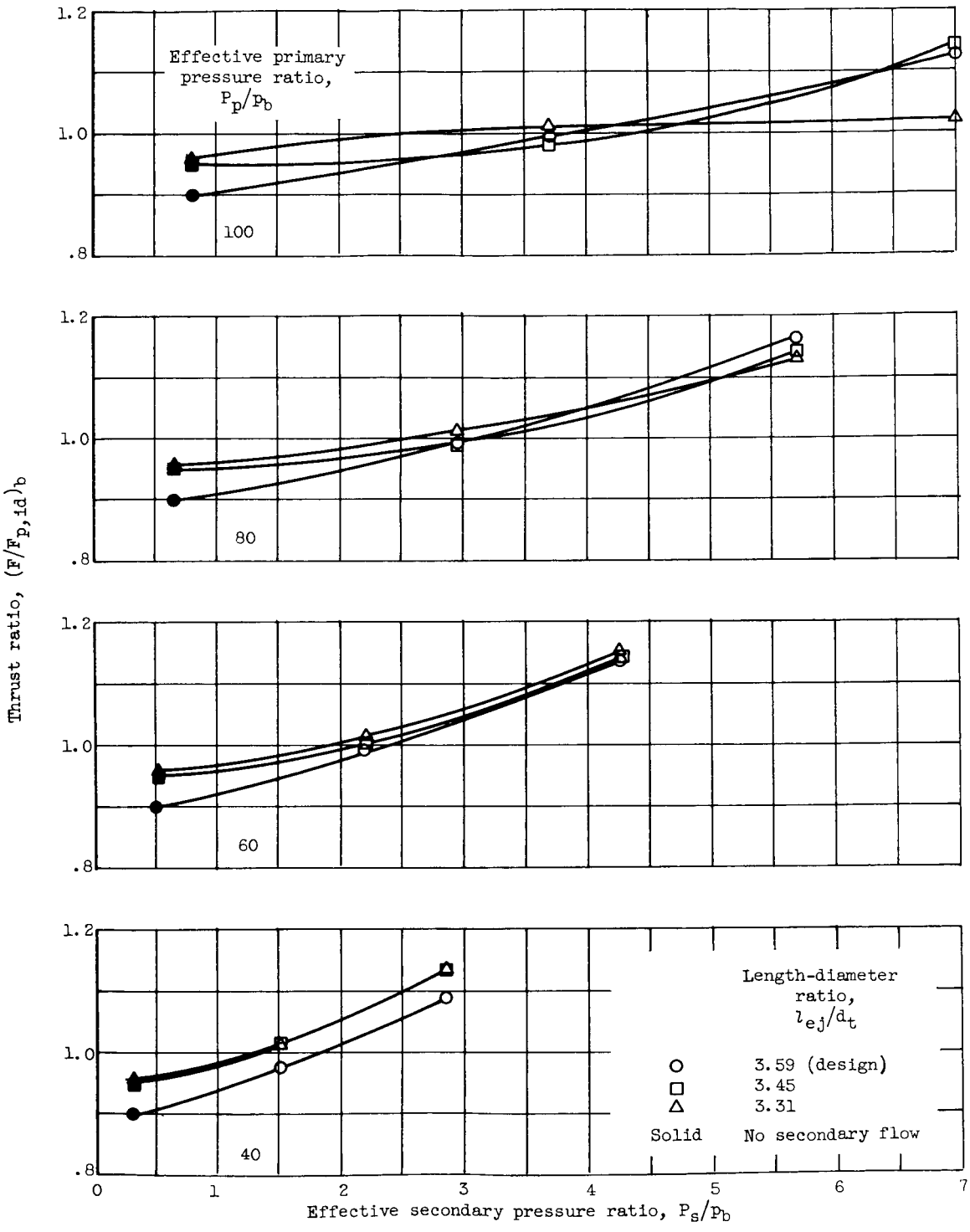


(b) Ejector diameter ratio, $d_s/d_t$, 3.25.

Figure 9. - Concluded. Calculated performance of ejector with conical primary nozzle in quiescent air.

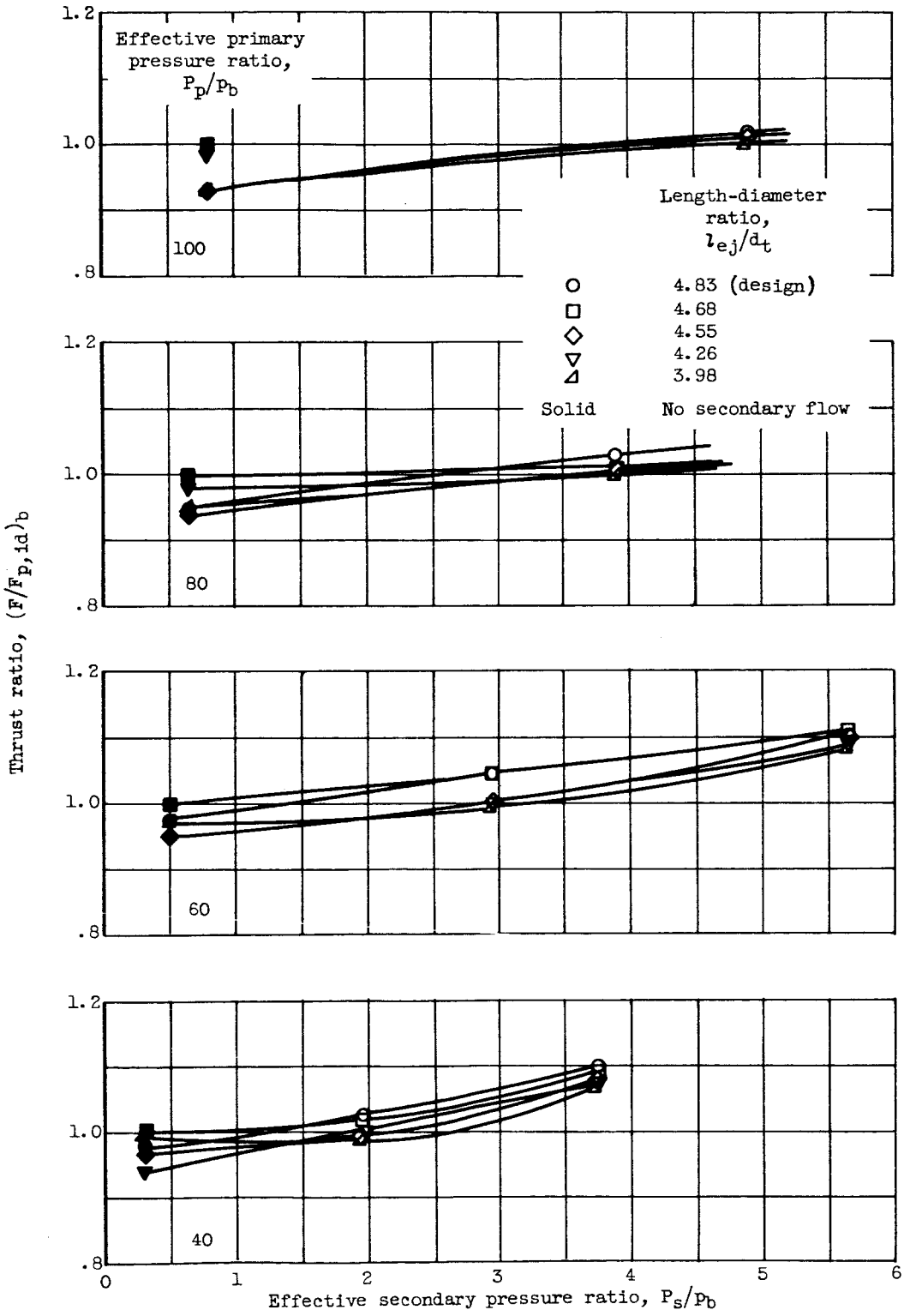


Figure 10. - Calculated performance of ejector with bell primary nozzle in quiescent air. Ejector diameter ratio, 2.82.

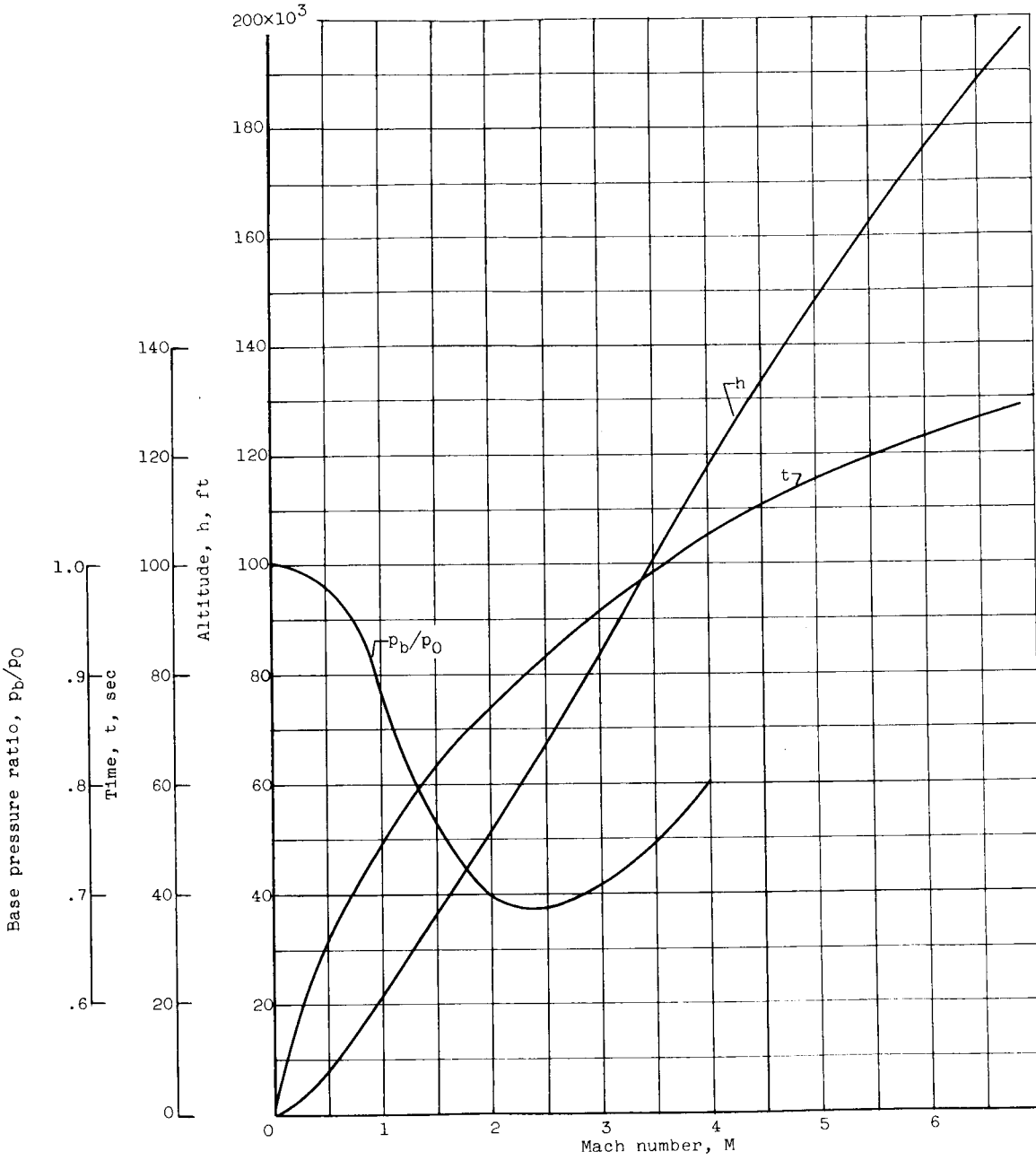


Figure 11. - Typical ballistic flight-path parameters.

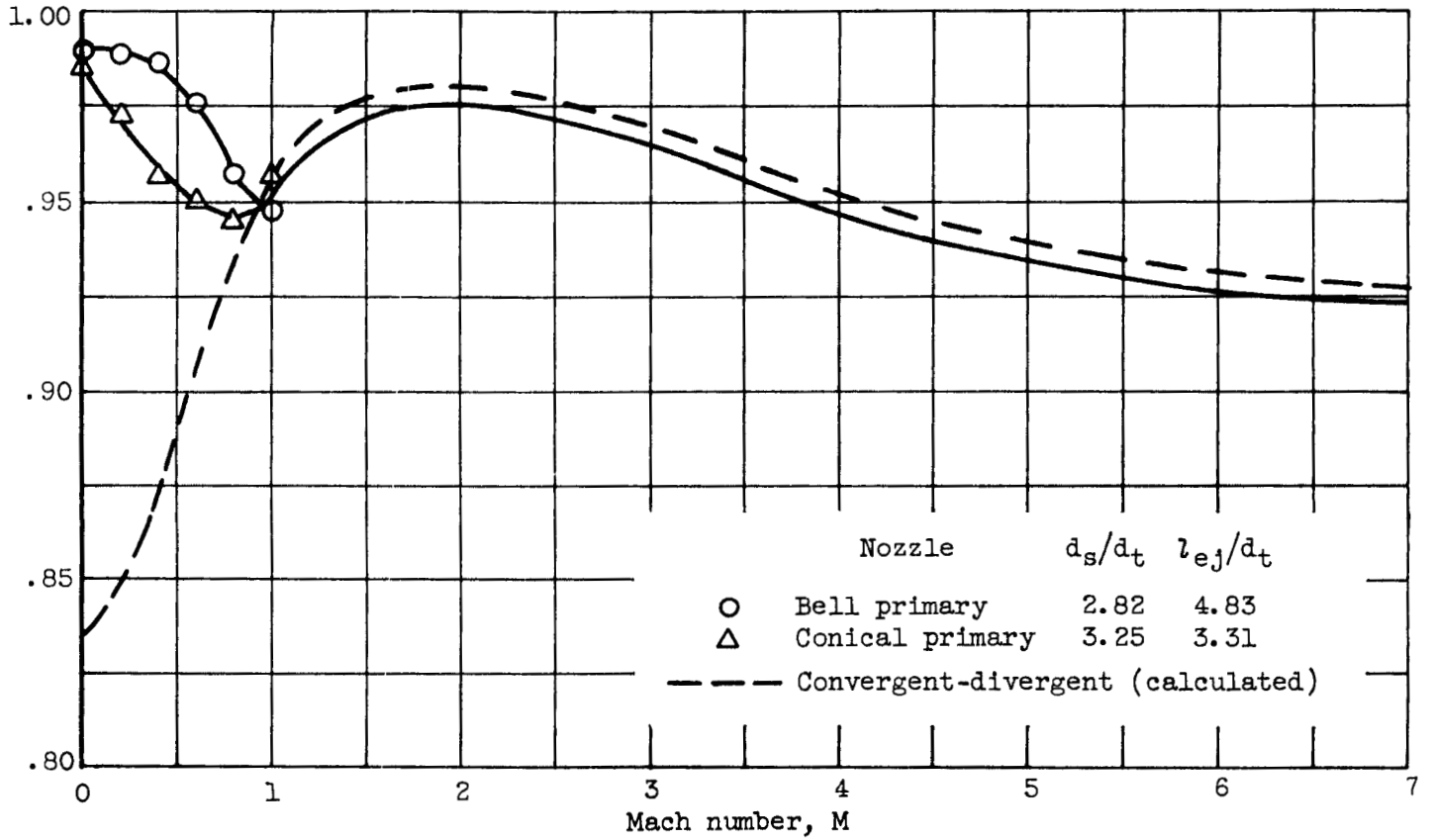


(a) Convergent-divergent nozzle with pressure ratio of 361.

Figure 12. - Performance comparison of ejector nozzles with two convergent-divergent nozzles over typical flight path. Primary total pressure, 650 pounds per square inch absolute.

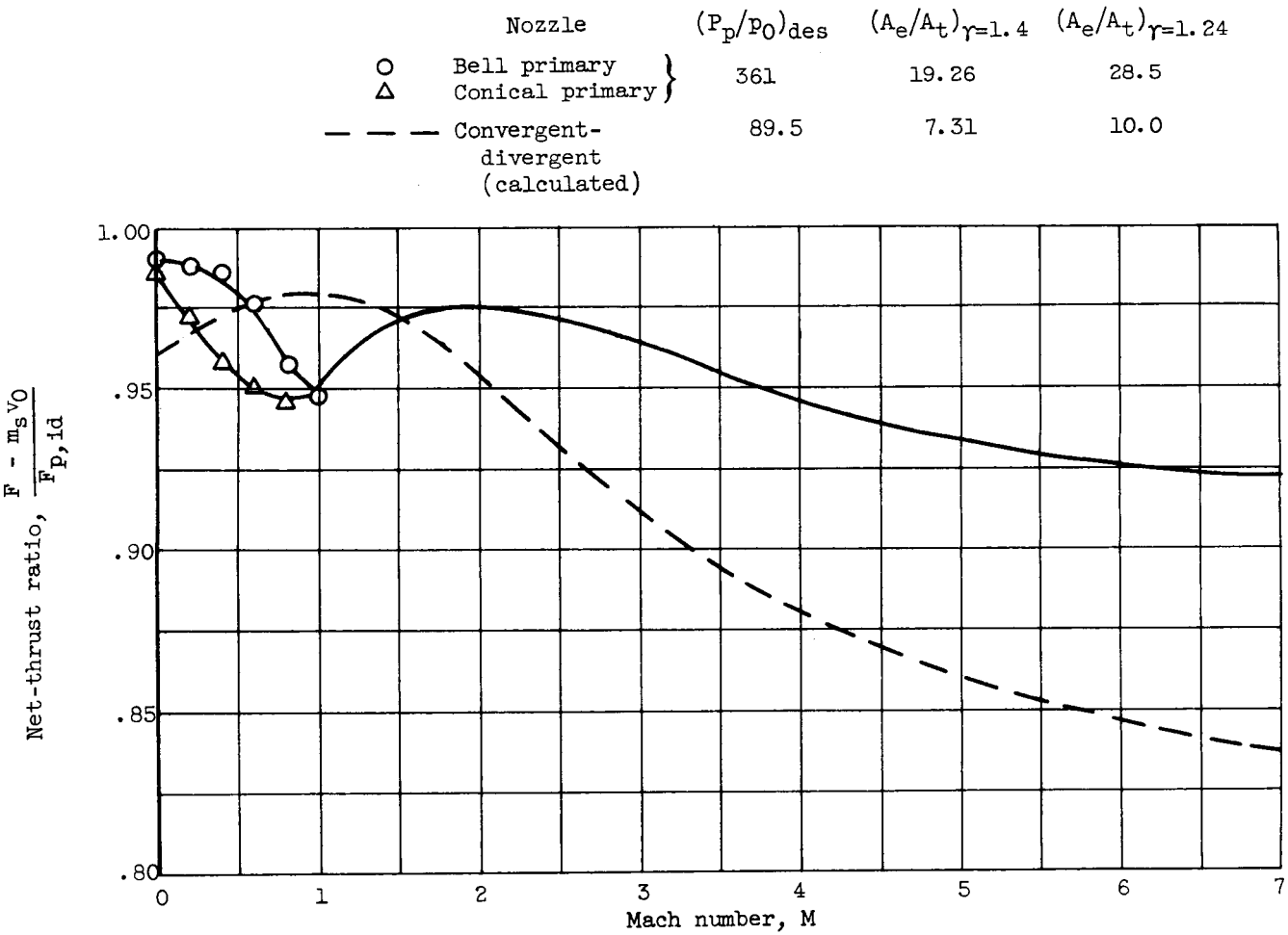


(b) Convergent-divergent nozzle with pressure ratio of 89.5.

Figure 12. - Continued. Performance comparison of ejector nozzles with two convergent-divergent nozzles over typical flight path. Primary total pressure, 650 pounds per square inch absolute.

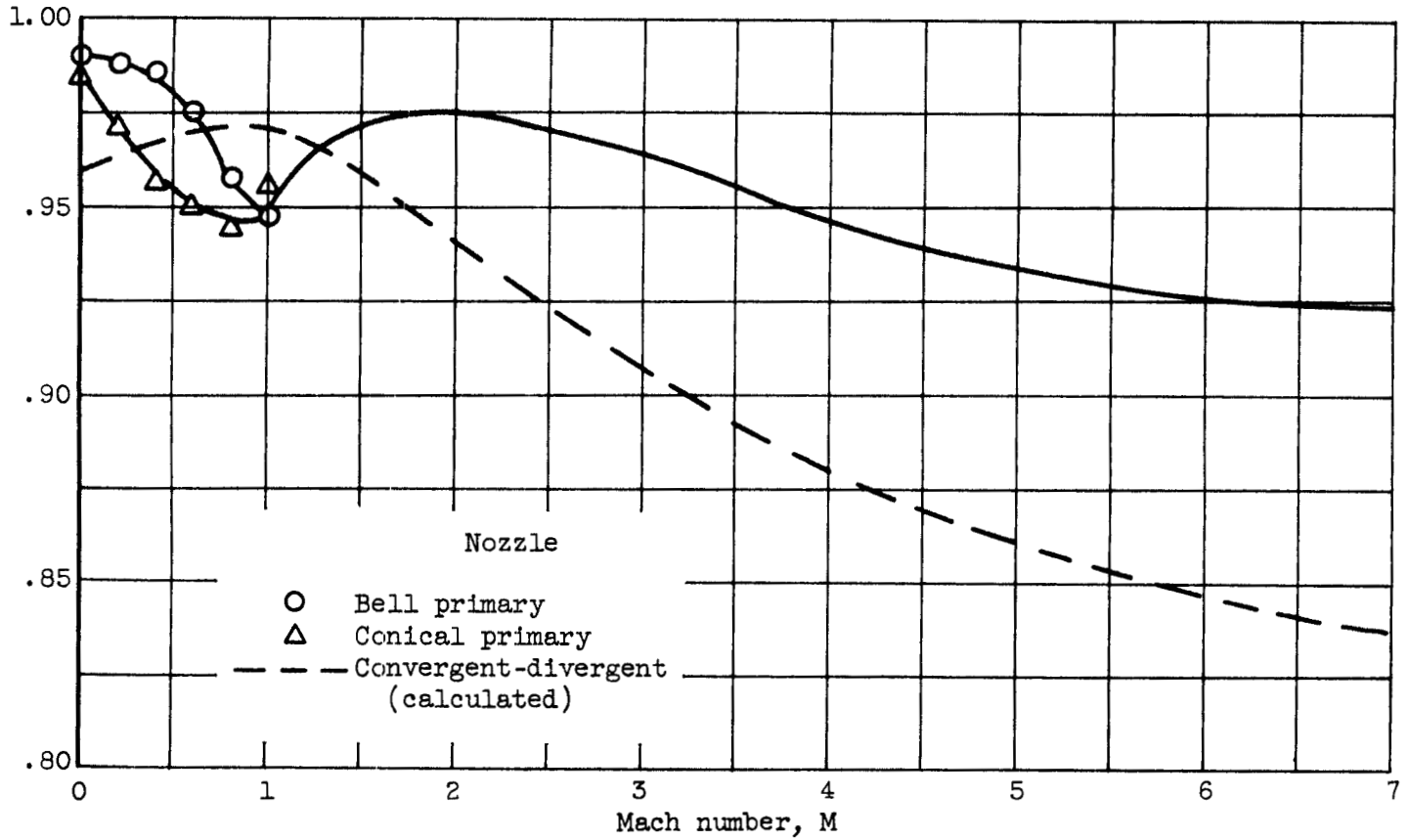


(c) Convergent-divergent nozzle with pressure ratio of 89.5 corrected for base drag caused by difference in exit areas.

Figure 12. - Concluded. Performance comparison of ejector nozzles with two convergent-divergent nozzles over typical flight path. Primary total pressure, 650 pounds per square inch absolute.

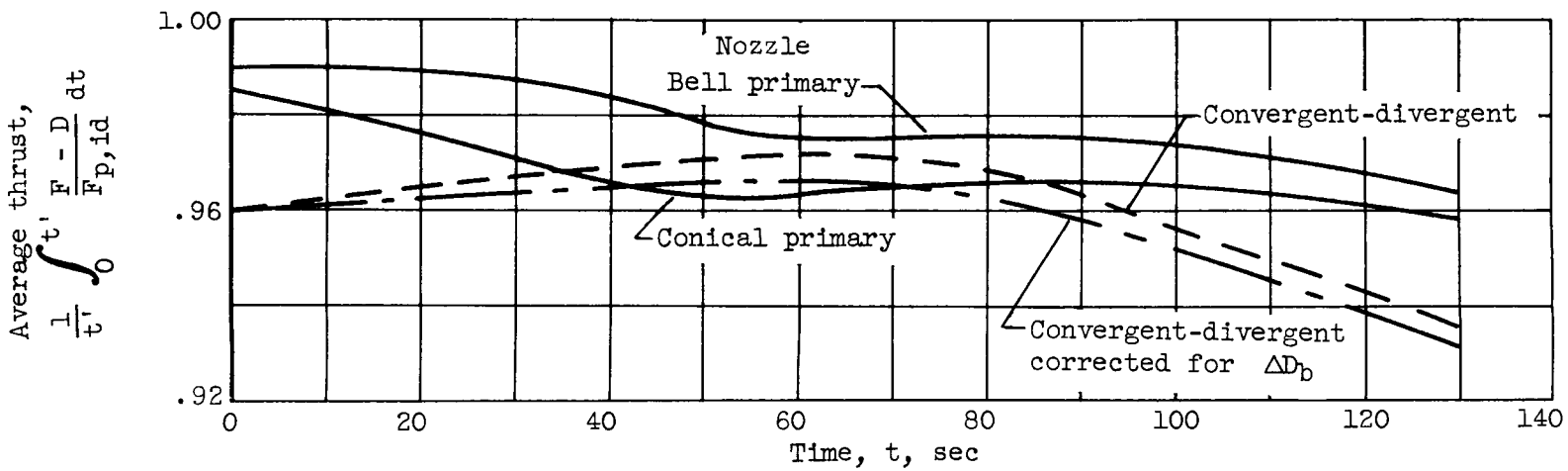


Figure 13. - Comparison of average thrust of ejector nozzles and convergent-divergent nozzle with pressure ratio of 89.5 over a typical flight path. Primary total pressure, 650 pounds per square inch absolute.